

## Advances in detecting $\alpha$ -dicarbonyl compounds: Insights from spectroscopic techniques

Xu Wu, Jing Wu, Jiawei Li, Yan Peng & Yiming Zhu

To cite this article: Xu Wu, Jing Wu, Jiawei Li, Yan Peng & Yiming Zhu (2024) Advances in detecting  $\alpha$ -dicarbonyl compounds: Insights from spectroscopic techniques, Applied Spectroscopy Reviews, 59:10, 1408-1434, DOI: [10.1080/05704928.2024.2335380](https://doi.org/10.1080/05704928.2024.2335380)

To link to this article: <https://doi.org/10.1080/05704928.2024.2335380>



Published online: 12 Apr 2024.



Submit your article to this journal [↗](#)



Article views: 183



View related articles [↗](#)



View Crossmark data [↗](#)



Citing articles: 1 View citing articles [↗](#)



## Advances in detecting $\alpha$ -dicarbonyl compounds: Insights from spectroscopic techniques

Xu Wu<sup>a</sup>, Jing Wu<sup>a,b</sup>, Jiawei Li<sup>a</sup>, Yan Peng<sup>a</sup>, and Yiming Zhu<sup>a</sup>

<sup>a</sup>Terahertz Technology Innovation Research Institute, Shanghai Key Lab of Modern Optical System, School of Optical-Electrical and Computer Engineering, University of Shanghai for Science and Technology, Shanghai, China; <sup>b</sup>College of Health Science and Engineering, University of Shanghai for Science and Technology, Shanghai, China

### ABSTRACT

The  $\alpha$ -dicarbonyl compounds are glycolysis metabolites with high reactivity that can cause damage to nucleic acids, proteins, and other macromolecules, leading to various chronic diseases. The rapid and accurate detection of  $\alpha$ -dicarbonyl compounds in organisms is of great significance for understanding their roles in the initiation and progression of chronic diseases. Spectroscopic techniques, known for their effectiveness, sensitivity, and ease of use, are widely employed for this purpose. This review provides a concise overview of the analytical strategies and performance of spectroscopic techniques used in detecting  $\alpha$ -dicarbonyl compounds, including nuclear magnetic resonance (NMR) spectroscopy, infrared (IR) spectroscopy, fluorescence spectroscopy, and ultraviolet-visible (UV-Vis) spectroscopy. Additionally, this review highlights the advancements and trends in the detection of  $\alpha$ -dicarbonyl compounds.

### KEYWORDS

$\alpha$ -dicarbonyl compounds; fluorescence spectroscopy; UV spectroscopy; IR spectroscopy; NMR spectroscopy

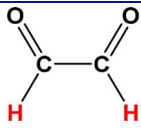
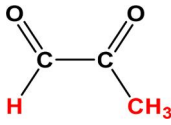
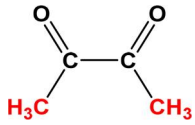
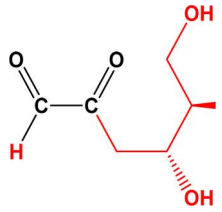
## Introduction

The  $\alpha$ -dicarbonyl compounds ( $\alpha$ -DCs) represent a distinct category of highly reactive electrophilic substances characterized by the presence of two carbonyl groups (C=O). This category comprises glyoxal (GO), methylglyoxal (MGO), 3-deoxyglucosone (3-DG), and 2,3-butanedione (2,3-BD). These compounds originate from two main sources: one is from food processing, particularly originating from high-sugar foods, such as cookies, cakes, yogurt, and honey.<sup>[1]</sup> The other source is the *in vivo* metabolic processes of carbohydrates, which include sugar degradation, lipid metabolism, and amino acid oxygenolysis.<sup>[2,3]</sup> Despite their origin in sugar, these compounds exhibit significantly higher activity, surpassing glucose by  $10^2$  to  $10^5$  times.<sup>[4]</sup>

Under normal circumstances,  $\alpha$ -DCs are carefully regulated by the glyoxalase enzyme system to maintain a healthy range in organisms. However, metabolic disorders can result in the abnormal accumulation of  $\alpha$ -DCs.<sup>[5]</sup> When concentrations of these compounds exceed the healthy range, they can lead to a multitude of unwanted bioeffects. Table 1 summarizes the unwanted biochemical changes caused by  $\alpha$ -DCs, highlighting

**CONTACT** Peng Yan  [py@usst.edu.cn](mailto:py@usst.edu.cn)  Terahertz Technology Innovation Research Institute, Shanghai Key Lab of Modern Optical System, School of Optical-Electrical and Computer Engineering, University of Shanghai for Science and Technology, Shanghai, China.

**Table 1.** Molecular structures and the main bioeffects of four representative  $\alpha$ -dicarbonyl compounds.

Name	Molecular structure	Bioeffect
Glyoxal (GO)		<ol style="list-style-type: none"> <li>1. <b>Superoxide anions:</b> inhibits the secretion of cytosolic oxidase, leading to cellular damage.<sup>[6]</sup></li> <li>2. <b>Genotoxic properties:</b> reacts with DNA and causes chromosomal mutations, promoting tumor activities.<sup>[7]</sup></li> </ol>
Methylglyoxal (MGO)		<ol style="list-style-type: none"> <li>1. <b>Oxidative stress:</b> has dual-role in cancer progression.<sup>[8,9]</sup> Lower doses of MGO are able to establish an adaptive response in cancer cells, while higher doses cause cellular apoptosis.<sup>[10,11]</sup></li> <li>2. <b>Major precursor of AGEs:</b> is implicated with diabetes, aging, neurodegenerative and cardiovascular diseases<sup>[5,12]</sup></li> </ol>
2, 3-Butanedione (2, 3-BD)		<ol style="list-style-type: none"> <li>1. <b>Oxidative stress:</b> impairs lung epithelial barrier function, potentially leading to bronchiolitis obliterans and even lung cancer.<sup>[13]</sup></li> <li>2. <b>Major precursor of AGEs:</b> reacts with hemoglobin and albumin, disrupting their normal functions and immune responses.<sup>[14]</sup></li> </ol>
3-Deoxyglucosone (3-DG)		<ol style="list-style-type: none"> <li>1. <b>Oxidative stress:</b> includes inflammation, oxidative stress, and the formation of AGEs disrupting mediating downstream effects.<sup>[15]</sup></li> <li>2. <b>Major precursor of AGEs:</b> glycolyzes IgG, thus interfering with its normal function and immunity, leading to diabetic microangiopathy.<sup>[16]</sup></li> </ol>

their crucial roles in human physiological processes. Their strong chemical reactivity carries substantial implications for cellular components, including nucleic acids, proteins, and lipids, leading to the formation of advanced glycation end products (AGEs) and oxidative stress-induced cellular damage.<sup>[17,18]</sup> Subsequently, these biochemical changes disrupt metabolic pathways, trigger the aberrant activation of inflammatory pathways,<sup>[19]</sup> and accelerate the abnormal proliferation and differentiation of cell,<sup>[20,21]</sup> leading to various chronic diseases such as cancer, neurological disorders, diabetes, and heart disease.<sup>[22–24]</sup>

These  $\alpha$ -dicarbonyl compounds are well-documented carcinogens and potent toxins in humans. Recent research has highlighted the clinical relevance of  $\alpha$ -DCs, particularly focusing on MGO. In 2012, Cai et al.<sup>[25]</sup> was observed that sustained exposure of mice to elevated concentrations of MGO led to the manifestation of hallmark symptoms of diabetes, including abdominal obesity and insulin resistance. Subsequently, in 2018, Hanssen et al.<sup>[26]</sup> identified a significant correlation between MGO levels and mortality rates in diabetic patients. More recently, further research uncovered the direct correlation between the levels of MGO in the blood of diabetic patients and the extent of vascular and neurological impairments, as well as the severe stenosis or complete occlusion of coronary arteries in both the heart and brain.<sup>[27,28]</sup> Beyond its implications in diabetes, elevated MGO levels were also noted in individuals afflicted with age-related conditions such as atherosclerosis,<sup>[29]</sup> renal failure,<sup>[30]</sup> Parkinson's disease,<sup>[31]</sup> and Alzheimer's disease.<sup>[32]</sup>

Given the diverse biogenic functions of  $\alpha$ -dicarbonyl compounds that impact various physiological and pathological processes, monitoring these compounds in organisms holds significant importance. This not only facilitates the identification and mitigation of potential health risks, but also enables the early diagnosis of conditions associated with the perturbations of these compounds.

### General methods for detecting $\alpha$ -dicarbonyl compounds

Because of the increasing attention to  $\alpha$ -dicarbonyl compounds in clinical medicine, various detection techniques have recently been developed. According to the Web of Science database (Figure 1a), 527 relevant articles published in the last decade (2012–2023). Among these, optical spectroscopic techniques, mass spectrometry,<sup>[33–35]</sup> electrochemical methods,<sup>[36,37]</sup> and enzyme-linked immunoassay (ELISA)<sup>[38,39]</sup> are commonly used. As shown in Figure 1b, optical spectroscopic techniques were the most popular (60.0% of related papers), followed by mass spectroscopy (27.3% of related papers). ELISA and electrochemical methods were less commonly used (<5% of related papers).

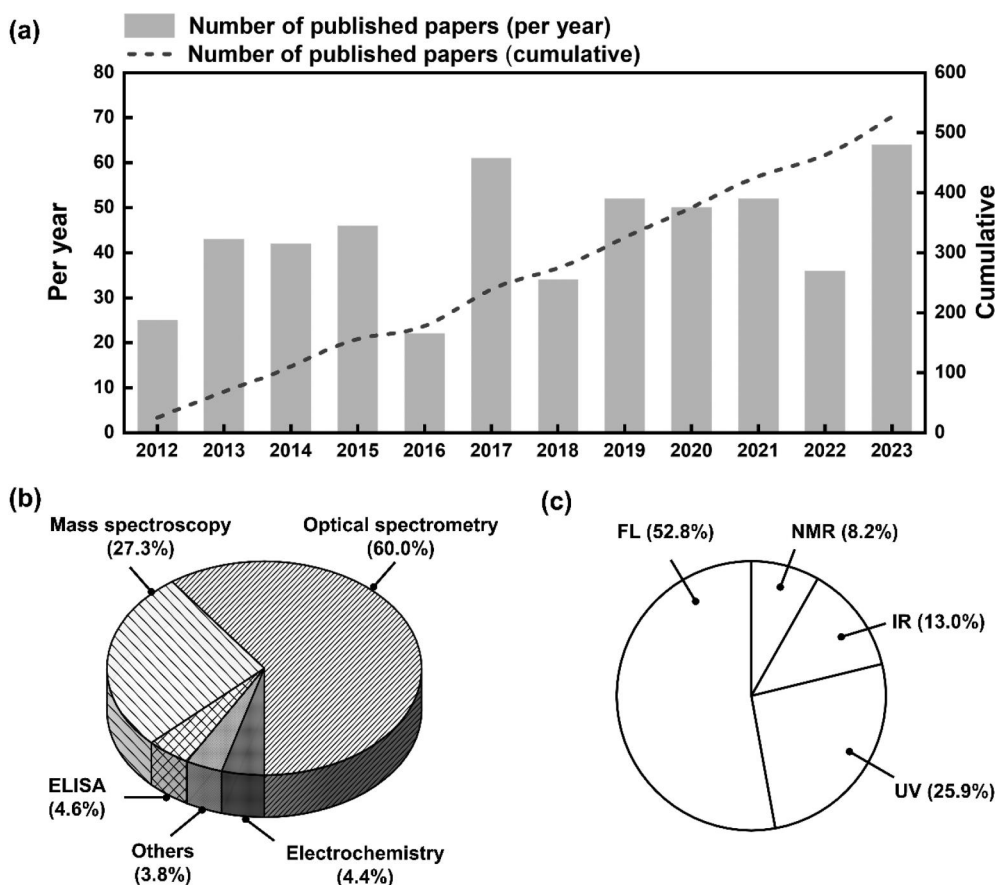


**Figure 1.** The number of published papers devoted to the determination of  $\alpha$ -dicarbonyl compounds in 2012–2023, according to Web of Science database.

Each of these technologies has advantages and disadvantages (Table 2). Electrochemical methods determine an analyte based on its electrical properties, such as potential, charge, and current. This method is low-cost and user-friendly, but it lacks specificity and sensitivity. To improve detection specificity, researchers have developed ELISA techniques, including competitive ELISA and sandwich ELISA, that rely on antigen-antibody interaction and enzymes. However, these methods require expensive labeled antibodies and lengthy pretreatment procedures, which limit their widespread use. Mass spectrometry is a powerful technique for detecting various organic compounds but it needs cost and complex instruments. In contrast to the aforementioned methods, optical spectroscopic techniques are based on the interaction between analyte and light (absorption, emission, and scattering).<sup>[40]</sup> Different spectroscopic techniques operate at different electromagnetic frequencies, but all offer high sensitivity, accuracy, rapid response time, low cost, as well as ease operation.<sup>[41,42]</sup> Therefore, despite many detection methods being used in  $\alpha$ -DCs analysis, optical spectroscopy techniques remain the most popular. In light of these, this review focuses on the analytical strategies and

**Table 2.** Overview of the advantages and disadvantages of spectrum detection and other frequently-used technologies in  $\alpha$ -dicarbonyl compounds detection.

Types	Technologies	Advantages	Shortages
Spectrum detection	FL probe	<ul style="list-style-type: none"> <li>• Visualization</li> <li>• Specificity</li> <li>• High sensitivity</li> <li>• High resolution imaging</li> </ul>	<ul style="list-style-type: none"> <li>• Requires specific labeling for target molecules</li> <li>• Limited penetration depth</li> <li>• Interference from background fluorescence</li> </ul>
	HPLC-FLD	<ul style="list-style-type: none"> <li>• High sensitivity</li> <li>• Specificity</li> </ul>	<ul style="list-style-type: none"> <li>• Requires specific labeling for target molecules</li> <li>• Interference from background fluorescence</li> </ul>
	LC-UV	<ul style="list-style-type: none"> <li>• Short wavelength for high resolution</li> </ul>	<ul style="list-style-type: none"> <li>• Cross-reaction with other compounds</li> <li>• time-consuming derivatization</li> <li>• variability induced by different sample treatments</li> </ul>
	NIR probe	<ul style="list-style-type: none"> <li>• High sensitivity</li> <li>• High selectivity</li> <li>• Real-time imaging for deep tissues</li> </ul>	<ul style="list-style-type: none"> <li>• Requires specific labeling for target molecules</li> </ul>
	MIR & FIR & THz	<ul style="list-style-type: none"> <li>• Simple operation</li> <li>• Suitable for chemical composition analysis</li> <li>• Nondestructive analysis</li> </ul>	<ul style="list-style-type: none"> <li>• Difficulty in complex overlapping peak analysis</li> <li>• Many interfering factors</li> <li>• Limited penetration in water-rich samples</li> </ul>
	NMR	<ul style="list-style-type: none"> <li>• Detailed information on molecular structures</li> <li>• Noninvasive analysis</li> </ul>	<ul style="list-style-type: none"> <li>• Expensive and complex instrument</li> <li>• Requires strong magnetic fields</li> <li>• Require professional data analysis</li> </ul>
Others	Electrochemistry	<ul style="list-style-type: none"> <li>• Low-cost</li> <li>• User-friendly operation</li> <li>• Rapid</li> </ul>	<ul style="list-style-type: none"> <li>• Interference from background sample composition</li> <li>• Limited sensitivity</li> </ul>
	ELISA	<ul style="list-style-type: none"> <li>• High specificity for target molecules</li> </ul>	<ul style="list-style-type: none"> <li>• Specific labeled antibodies are required</li> <li>• Time-consuming</li> <li>• Interference from sample matrix</li> </ul>
	Mass spectrometry	<ul style="list-style-type: none"> <li>• High sensitivity</li> <li>• Identifies and quantifies complex mixtures</li> </ul>	<ul style="list-style-type: none"> <li>• Expensive equipment and maintenance costs</li> <li>• Destructive and Cumbersome sample preparation process</li> <li>• Requires long-running</li> </ul>

performance of different spectroscopic detections used in determining  $\alpha$ -DCs, along with their advances and trends.

## Optical spectroscopic techniques for detecting $\alpha$ -dicarbonyl compounds

Optical spectroscopy techniques serve as guiding tools for revealing the diverse nature of  $\alpha$ -DCs across different electromagnetic waves, as shown in Figure 2. From 2012 to 2023, many research groups have used optical spectroscopy techniques to analyze  $\alpha$ -DCs. According to the Web of Science database (Figure 1c), 248 relevant articles were published. Fluorescence (FL)-based methods were the most popular (52.8% of related

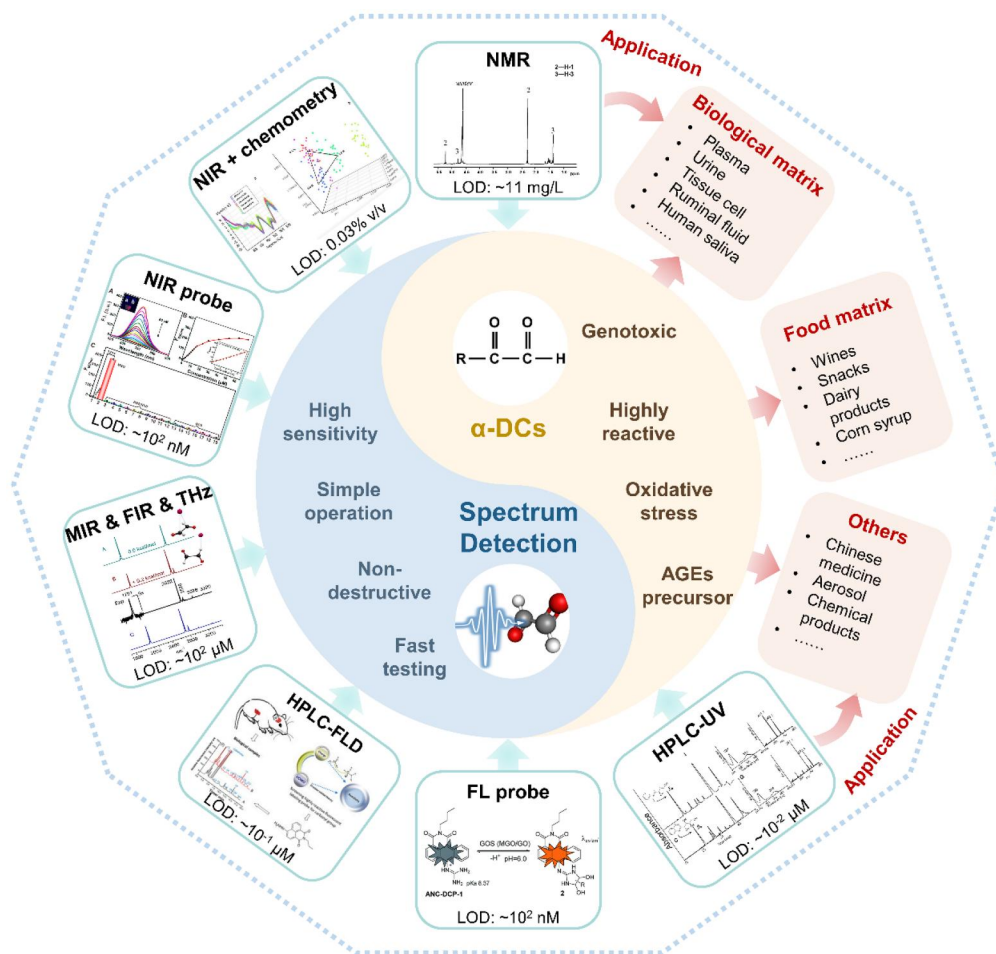


**Figure 2.** Framework of the review on recent advancements in optical spectroscopy techniques for  $\alpha$ -dicarbonyl compounds analysis, including fluorescence (FL), ultraviolet (UV), infrared (IR), and nuclear magnetic resonance (NMR) spectroscopy. Adapted with permission from Ref.<sup>[43]</sup> © 2014 American Chemical Society. Adapted with permission from Ref.<sup>[44]</sup> © 2018 Elsevier B.V. Adapted with permission from Ref.<sup>[45]</sup> © 2015 Elsevier B.V. Adapted with permission from Ref.<sup>[46]</sup> © 2019 American Chemical Society. Adapted with permission from Ref.<sup>[47]</sup> © 2004 Elsevier Inc. Adapted with permission from Refs.<sup>[48,49]</sup> All article content, except where otherwise noted, is licensed under a Creative Commons Attribution (CC BY) license.

papers), followed by ultraviolet (UV) spectroscopy (25.9% of related papers), infrared (IR) spectroscopy (13.0% of related papers), and nuclear magnetic resonance (NMR) spectroscopy (8.2% of related papers). These spectroscopic techniques have been used in various applications such as food, biological samples, aerosols, and pharmaceuticals. Each of these techniques will be discussed in detail.

### **Ultraviolet spectroscopy detection**

Our investigation begins with UV spectroscopy, which exposes the electronic transitions occurring within  $\alpha$ -DCs in the wavelength range of 10 to 400 nm. The detection principle is as follows: each  $\alpha$ -dicarbonyl compound possesses two carbonyl groups (C=O), containing conjugated  $\pi$  electrons that absorb UV radiation. By analyzing the wavelength and intensity of UV peaks, we can directly identify and characterize these organic molecules. The application of ultraviolet spectroscopy in detecting  $\alpha$ -carbonyl compounds can be categorized into two classes: direct UV detection and liquid chromatogram (LC)-UV detection, where UV spectroscopy is combined with LC.

#### **Direct UV detection**

The UV spectra of  $\alpha$ -carbonyl compounds are influenced by their molecular structures and surrounding microenvironments (solvent polarity, pH, temperature, and complexing agents). Since the 1990s, UV spectroscopy has been used to analyze the molecular structure of  $\alpha$ -carbonyl compounds. For instance, Meller et al.<sup>[50]</sup> used conventional UV spectroscopy to analyze gas-phase MGO and found it exhibits high cross-sectional values within the range of 370 to 450 nm. In 1998, Koch et al.<sup>[51]</sup> employed home-made UV spectroscopy to monitor MGO and further investigate its photolysis in air. They identified two  $n\text{-}\pi^*$  transition peaks at 290 nm and 445 nm respectively. These works contributed to our understanding of MGO behavior in the UV region and provided valuable insights into its monomer structure. In 2005, Volkamer et al.<sup>[52]</sup> conducted a high-resolution UV measurement for GO and reported UV absorption values that were 10–30% higher at 250 nm and 526 nm compared to previous low-resolution works. This research enhanced calculations related to GO dissociation frequency and improved wavelength calibration accuracy. These studies have provided a valuable database for analyzing the molecular structures of  $\alpha$ -carbonyl compounds through UV spectroscopy.

Also, UV spectroscopy plays an important role in the microenvironmental analysis of  $\alpha$ -carbonyl compounds. Nemet et al.<sup>[47]</sup> investigated the effect of solvent and temperature on MGO through direct UV detection. Within different solvents, the UV absorption peak of MGO remained at 290 nm while the intensity varied. After dehydration of MGO, an absorption peak at 430 nm appeared, and disappeared after re-addition of water. These findings indicate that MGO exhibits two different forms: the 290 nm peak is associated with the monomer form, while the 430 nm peak is linked to the polymer form. Furthermore, it is evident that the solution has a significant influence on the equilibrium between different MGO structures. In addition, heating MGO at 60 °C for 30 mins increased the intensity at 290 nm, suggesting a temperature-induced alteration in carbonyl forms.

### **LC-UV detection**

However, the high reactivity of  $\alpha$ -DCs easily leads to interference in their direct UV detection, posing challenges for precise analysis in organisms. To address this problem, the combination of UV spectroscopy and LC technique provides a reliable approach by facilitating their separation from interfering substances using LC and enabling precise quantification through UV detection based on their UV chromophores.

The development of HPLC-UV techniques for the analysis of  $\alpha$ -DCs in various organisms has undergone significant progress over time. Table 3 summarizes the representative works. In the work conducted by Nemet et al.<sup>[53]</sup> in 2004, reverse-phase HPLC with UV detection was used to detect MGO in human plasma. This approach involved protein precipitation and derivatization treatment using 1,2-diamino-4,5-dimethoxybenzene, offering advantages of cost-effectiveness and rapidity. The linear concentration range covered 200 to 1000 nmol/L, with a limit of detection (LOD) of 30.6 pmol at 215 nm and a relative standard deviation (RSD) of 3.5%. In 2018, Wang et al.<sup>[54]</sup> successfully employed HPLC-UV detection to quantify four  $\alpha$ -dicarbonyl compounds (GO, MGO, 3-DG, and 2, 3-BD) in commonly consumed foods. The derivatization was conducted with 4-(2,3-dimethyl-6-quinoxaliny)-1,2-benzenediamine, at pH 9.0 and ambient temperature for 30 mins. This method demonstrated low LODs (0.05  $\mu$ mol/L for GO, 0.05  $\mu$ mol/L for MGO, 0.05  $\mu$ g/L for 3-DG, and 0.02  $\mu$ mol/L for 2,3 BD), and an RSD below 2.7%. In 2020, Taibi et al.<sup>[57]</sup> used reverse-phase HPLC-UV detection to analyze the MGO level in cattle serum, employing o-phenylenediamine as the derivatization agent. This method exhibited a linear range of 4.2–422  $\mu$ g/mL, with the LOD of 51.41  $\mu$ g/mL and the limit of quantification (LOQ) of 155.80  $\mu$ g/mL. The precision as indicated by the RSD, remained below 7.15%. These works demonstrated that the LC-UV detection methods offer a dependable and effective approach for quantifying  $\alpha$ -DCs in biosamples, providing valuable insights into food chemistry and glucose metabolism.

In short, UV spectroscopy is a simple way to detect  $\alpha$ -DCs, but its effectiveness is limited for complex organisms. Combining it with LC improves sensitivity and selectivity, but requires extra steps like derivatization. Nonetheless, challenges remain in HPLC-UV due to reliance on OPD derivatization, which can be interfered with by other compounds. Additionally, derivatization and separation processes are time-consuming, limiting the use for monitoring changes in complex samples. More importantly, different sample treatments such as complex lysis procedures in cell studies, lead to variability in results. Therefore, developing new derivatization agents to enhance selectivity and reduce time, along with establishing standardized sample treatment protocols, are crucial for advancing LC-UV technology in  $\alpha$ -DCs analysis.

### **Fluorescence spectroscopy detection**

Fluorescence spectroscopy is a prominently employed technique for analyzing the structure, conformation, and microenvironment of biomolecules through the measurement of their fluorescent emission, typically within the visible range (200–700 nm). The identification of molecular species is facilitated by the dependence of the position and shape of fluorescent peaks on the electronic structure within molecules. Changes in concentration or environment can be inferred by examining the fluorescence intensity, which

**Table 3.** LC-UV with different derivatives for  $\alpha$ -dicarbonyl compounds detection.

Derivatization reagent	Experimental procedure	Biological matrix	Detection limit	Repeatability (RSD <sup>†</sup> )	References
1,2-diamino-4,5-dimethoxybenzene (DOB)	pH: <7 Temp: 25 °C Time: 4 hours Detection: UV (352 nm)	Human plasma	LOD <sup>‡</sup> : 30.6 pmol	<3.5%	Nemet et al. <sup>[53]</sup>
4-(2,3-dimethyl-6-quinoxalyl)-1,2-benzenediamine (DOB)	pH: 9 Temp: RT <sup>†</sup> Time: 30 mins Detection: UV (254 nm)	Commonly consumed foods Human saliva	LOD: <0.05 $\mu$ M LOQ <sup>‡</sup> : <0.20 $\mu$ M LOD: <0.05 $\mu$ M LOQ: <0.20 $\mu$ M	0.12–2.7% 0.35–1.7%	Wang et al. <sup>[54]</sup> Wang et al. <sup>[55]</sup>
o-phenylenediamine (OPD)	pH: 6, acetate buffer Temp: RT Time: overnight Detection: UV (254 nm) pH: <7, 0.45M HClO <sub>4</sub> Temp: RT Time: 48 hours (in dark) Detection: UV (313 nm) pH: 7, HEPES buffer Temp: RT Time: 2–4 hours (in dark) Detection: UV (316 nm) pH: 7, sodium phosphate buffer Temp: RT Time: overnight Detection: UV (312 nm) pH: 6.5, phosphate buffer Temp: RT Time: 16 hours (in dark) Detection: UV (312 nm) pH: 6.5, sodium phosphate buffer Temp: RT Time: overnight Detection: UV (312 nm) pH: N. A. Temp: RT Time: 24 hours (in dark) Detection: UV (315 nm)	Diabetic plasma Methionine oxidation products  Cattle serum  Corn sirup  Commonly consumed foods  Simulated gastrointestinal digestion  Commonly commercial wines  Liver Plasma Vascular smooth muscle cells	LOD: 0.1 $\mu$ M LOD: 2.9 $\mu$ M  LOD: 51.41 $\mu$ g/mL LOQ: 155.8 $\mu$ g/mL  LOD: <12.2 ng/mL LOQ: <40.2 ng/mL  LOD: <1.49 mg/kg  LOD: /  LOD: 0.9 mg/L  LOD: 0.01 $\mu$ M LOQ: 0.05 $\mu$ M	1.28–5.69% N. A.  7.15%  <6.5%  <7.5%  N. A.  N. A.  1.70%	Wang et al. <sup>[56]</sup> Hellwig et al. <sup>[43]</sup>  Taibi et al. <sup>[57]</sup>  Gensberger et al. <sup>[58]</sup>  Degen et al. <sup>[59]</sup>  Treibmann et al. <sup>[60]</sup>  Kertsch et al. <sup>[61]</sup>  Dhar et al. <sup>[62]</sup>

<sup>†</sup>RSD: relative standard deviation (intra-day); LOD: limit of detection; LOQ: limit of quantification; RT: Room temperature; N. A.: not mentioned in the literature.

depends on the excited state lifetime and molar absorption rate. This method finds broad application in environmental, pharmaceutical, and biological analyses. However, direct detection of  $\alpha$ -DCs poses a challenge owing to their absence of inherent fluorescence properties. Therefore, diverse labeling techniques are employed in the fluorescence spectroscopy detection of  $\alpha$ -DCs,<sup>[63,64]</sup> which can be classified into two main types: derivatization reaction-based or probe-based methods.

### **Derivatization reaction-based fluorescence detection**

Table 4 presents the commonly used derivatizing agents for detecting  $\alpha$ -dicarbonyl compounds through fluorescence analysis. In a study by Lodge-Ivey et al.,<sup>[65]</sup> high-performance liquid chromatography-fluorescence technique (HPLC-FLD) was employed to analyze MGO in rumen fluid, using the derivatizing agent 6-hydroxy-2,4,5-triaminopyrimidine (TRI). This method demonstrated a LOD of 0.125  $\mu\text{g/mL}$ , accompanied by an intraday RSD of 4.7%. The approach determined the MGO levels in urine from various subjects, showcasing its sensitivity and effectiveness. In 2014, Ojeda et al.<sup>[66]</sup> determined different  $\alpha$ -dicarbonyl compounds (GO, MGO, and 2, 3-BD) in urine using HPLC-FLD with the derivatizing agent of 4-methoxy-*o*-phenylenediamine (4-MPD). This method achieved baseline resolution within 12 mins, demonstrating its time-saving characteristic. The LODs for GO, MGO, and 2,3-BD were found to be 0.46  $\mu\text{g/L}$ , 0.39  $\mu\text{g/L}$ , and 0.28  $\mu\text{g/L}$ , respectively, with an intraday RSD of 6%, demonstrating its high-sensitive and precise characteristics. This approach is supposed to be applied in clinical-related studies. In 2015, Rodríguez-Cáceres et al.<sup>[67]</sup> applied HPLC-FLD to quantify GO and MGO in wine, using 3,4-diaminopyridine as a derivatization reagent. This method offered advantages of rapid separation (about 4 min) and high sensitivity (LOD: 1.29  $\mu\text{g/L}$  for GO and 0.44  $\mu\text{g/L}$  for MGO). In 2016, a study led by Ogasawara et al.,<sup>[68]</sup> the concentration of MGO in human plasma was measured following a 40-min reaction with 1,2-diamino-4,5-methylenedioxybenzene (DMB) through HPLC-FLD. The results indicated that MGO levels in human plasma ranged from 24 to 258 nmol/L, with an RSD value of 2.55%. In 2019, Dhananjayan et al.<sup>[69]</sup> employed ultra-high-performance liquid chromatography (UHPLC) coupled with fluorescence detection for the determination of GO and MGO in serum samples. The derivatization reagent was 6-diamino-2,4-dihydropyrimidine sulfate (DDP). The achieved LODs were 0.17 pmol for GO and 0.10 for MGO respectively, with an intraday RSD below 7.3%.

The derivatizing agents can be divided into three types. The first type includes fluorescent derivatives with a specific structure that reacts with MGO to form a stable ring structure and emit fluorescence for selective detection. Examples include DMN, TRI, 4-MPD, 3,4-DAP, DMB, and DDP. Their differences are mainly in reaction conditions, such as temperature, derivatization time, and pH, making them suitable for different biological matrix detection applications. 4-MPD has the longest derivatization time (4 h) and a low reaction temperature (40 °C), making it stable and suitable for repetitive detection in neutral matrices. DMN, TRI, and DMB have shorter derivatization times (<1 h) and faster elution separation speeds (10 min), but require a slightly higher reaction temperature (60–80 °C) and acidic pH. Therefore, these derivatizing agents are suitable for rapid detection in acidic biological matrices, while lower temperature and alkaline pH are suitable for fast detection in alkaline biological matrices. DDP can react

**Table 4.** HPLC-FLD with different derivatives for  $\alpha$ -dicarbonyl compounds detection.

Derivatization reagent	Experimental procedure	Biological matrix	Sensitivity (LOD <sup>†</sup> )	Repeatability (RSD <sup>†</sup> )	References
N-propyl-4-hydrazino-1,8-naphthalimide (NPHNA)	Temp: RT <sup>†</sup> Time: 1 hours pH: <7, phosphoric acid Detection: fluorescence (436/546 nm) Temp: 80 °C	Aliphatic aldehydes	0.29 nmol/L	2.79%	Chen et al. <sup>[44]</sup>
2,3-Diaminaphthalene (DMN)	Time: 50 mins pH: 6 Detection: fluorescence (276/500 nm) Temp: 60 °C	Traditional Chinese medicines	<1.04 × 10 <sup>-2</sup> μM	<2.75%	He et al. <sup>[64]</sup>
6-hydroxy-2, 4, 5-triaminopyrimidine (TRI)	Time: 45 mins pH: <7, 0.02M CH <sub>3</sub> COONa Detection: fluorescence (352/447 nm) Temp: 40 °C	Ruminal fluid	0.125 μg/mL	4.70%	Lodge-Ivey et al. <sup>[65]</sup>
4-methoxy-o-phenylenediamine (4-MPD)	Time: 4 hours pH: 7.4, phosphate buffer Detection: fluorescence (344/420 nm) Temp: 90 °C	Urine	0.39 μg/L	<6%	Ojeda et al. <sup>[66]</sup>
3,4-diaminopyridine (3,4-DAP)	Time: 120 mins pH: >7, 0.3M ClCH <sub>2</sub> COOH/C <sub>2</sub> H <sub>5</sub> ClNaO <sub>2</sub> Detection: fluorescence (307/471 nm) Temp: 60 °C	Wines	0.045 μg/L	2.90%	Rodríguez-Cáceres et al. <sup>[67]</sup>
1,2-diamino-4,5-methylenedioxybenzene (DMB)	Time: 40 mins pH: 1.0M C <sub>2</sub> H <sub>6</sub> O <sub>5</sub> /28mM Na <sub>2</sub> O <sub>5</sub> Detection: fluorescence (355/393 nm) Temp: 60 °C	Plasma	6 fmol/μL	2.55%	Ogasawara et al. <sup>[68]</sup>
5,6-diamino-2,4-dihydropyrimidine (DDP)	Time: 2 hours pH: 7.6, sodium phosphate buffer Detection: fluorescence (320 nm) Temp: 60 °C	Serum	0.1 pmol	<7.3%	Dhananjayan et al. <sup>[69]</sup>
2,2'-fural	Time: 30 mins pH: >10 Detection: fluorescence (330/450 nm) Temp: 90 °C	Wine	0.02 ng/mL	<6%	Hurtado-Sánchez et al. <sup>[70]</sup>
	Time: 30 mins pH: 3M CH <sub>3</sub> COONH <sub>4</sub> Detection: fluorescence (250/355 nm)	Human sera	0.1 nmol/mL	<5%	El-Maghrabey et al. <sup>[71]</sup>

<sup>†</sup>RSD: relative standard deviation (intra-day); LOD: limit of detection; RT: Room temperature.

with dicarbonyl compounds in both acidic and alkaline conditions, making it adaptable to various biological matrices by adjusting the pH.

In addition to fluorescent derivatives, there are hydrazine-based and furan-based derivatives. Hydrazine-based derivatives like NPHNA react easily with MGO without heating but have lower bio-safety. Furan-based derivatives like 2,2'-furyl are safer and more efficient but need a higher reaction temperature.

### **Fluorescent probe technology**

Unlike derivatization-based fluorescence detection, fluorescence probe technology involves the attachment of fluorescent probes to target molecules, facilitating selective recognition. When target molecules are excited by an external light source, the attached fluorescence probe emits a signal at a distinct wavelength. Through analyzing the intensity, wavelength, and lifetime of this fluorescence signal, both qualitative and quantitative identification of the target molecule can be achieved. This technology presents the benefits of real-time observability, robust specificity, noninvasiveness, and superior spatial and temporal resolution. Therefore, it is widely used for analyzing the concentration and environmental factors related to target molecules. In 2013, Wang et al.<sup>[72]</sup> reported a one-photon fluorescent probe named MBo (methyl diaminobenzene-BODIPY) to visualize MGO levels within live cells. This fluorescent probe distinguished itself by overcoming the electron-deficient nature of quinoxalines through strategically optimizing both the fluorophore and aromatic group electronics in reaction to MGO. Notably, this probe exhibited high sensitivity and exceptional selectivity in *in vitro* experiments, demonstrating effectiveness even at low concentrations (50 nM). Meanwhile, this approach simplified sample processing (without the need for protein precipitation steps) and significantly reduced incubation time (3 h as opposed to 24 h). This innovative tool was considered to be of great value for unraveling the intricate roles of MGO in various diseases and cellular processes.

However, single emission wavelength fluorescent probes face challenges in biological tissue analysis due to their susceptibility to absorption and autofluorescence interference in tissues, potentially compromising detection accuracy. Recently, ratiometric fluorescent probes have garnered significant research interest. In 2015, Tang et al.<sup>[73]</sup> introduced PDN-1, a two-photon "turn-on" fluorescence probe designed for the rapid detection of MGO. This probe is characterized by its dual interaction with both MGO and the OPD group, resulting in a remarkable 33-fold increase in fluorescence by inhibiting photoconductive electron transfer. The enhanced fluorescence enabled a LOD of 77 nM within the range of 0–10  $\mu\text{M}$ . In 2021, Wang et al.<sup>[74]</sup> reported a ratiometric fluorescent probe named NAP-DCP-4 for MGO detection in cells. This probe introduced OPD and guanidine (GND) as bipolar reaction sites, forming an "AND" logic gate system. Differing from the probe designed by Tang et al.,<sup>[73]</sup> NAP-DCP-4 exhibited remarkable reversibility with MGO, attributed to its ingenious design that harnessed the intramolecular charge transfer mechanism and the excitation wavelength modulation to selectively induce fluorescence emission from deprotonated adducts. This distinctive attribute significantly improved selectivity for MGO compared to other dicarbonyl compounds, resulting in a noteworthy LOD of 1.8  $\mu\text{M}$ . With this tool, the changes in MGO levels within the RAW264.7 cells after lipopolysaccharide stimulation were successfully

monitored. In 2022, Wang et al.<sup>[48]</sup> accomplished a breakthrough in the simultaneous determination of different  $\alpha$ -DCs. They introduced an open fluorescent probe (ANC-DCP-1) for monitoring MGO and GO in urine, achieving impressive LODs of 7.3  $\mu\text{M}$  for MGO and 4.7  $\mu\text{M}$  for GO, respectively. More recently, Xie et al.<sup>[75]</sup> specifically designed a fluorescence probe (2,3-diaminonaphthalene, DAN), for monitoring MGO levels in blood samples from diabetes subjects. With increasing MGO concentration, the fluorescence intensity of DAN gradually diminishes, while the intensity of the DAN-MGO adduct proportionally increases, as visually represented by a progressive shift in fluorescence color from blue to green. One significant feature of this probe is its exceptional detection efficiency. Within just 60 min, the fluorescence intensity of DAN rapidly decreases by approximately 100%, while there is a simultaneous and substantial increase in product fluorescence intensity. Another significant feature of this probe is its high sensitivity, with a LOD of 0.33  $\mu\text{M}$ . The fluorescence intensity is noteworthy for its strong correlation with MGO concentration in the range of 0–75  $\mu\text{M}$ , supported by an impressive correlation coefficient of 0.991. In addition to its sensitivity, the method demonstrates remarkable specificity for MGO and exceptional resilience against interference. A comparative analysis with the traditional OPD probes revealed the inherent self-correction capabilities of the ratiometric strategy. DAN strategically evades interference from serum and intracellular medium through the emission peak at 530 nm for DAN-MGO adduct formation.

Researchers encounter three main challenges when detecting  $\alpha$ -DCs with fluorescent probes. At first, the majority of documented fluorescent probes are designed for the selective detection of methylglyoxal (MGO), utilizing ortho-phenylenediamine (OPD) as the reactive moiety. While OPD demonstrates enhanced reactivity with MGO under physiological conditions in comparison to other alpha-dicarbonyls, thereby effectively mitigating cross-reactivity, it is prone to nonspecific reactions with other reactive species such as formaldehyde (FA) and nitric oxide (NO). Additionally, a significant portion of fluorescent probes necessitate prolonged reaction times, rendering them unsuitable for applications in tissue imaging or real-time monitoring. Lastly, the irreversible reactivity exhibited by most probes poses a challenge in dynamically tracking the levels of  $\alpha$ -DCs.

To address these issues, researchers developed efficient, selective, and reversible fluorescent probes by combining the OPD group with other fluorescent groups. [Table 5](#) compares these probes in DCs detection, including optimum detection conditions, Sensitivity, and selectivity. Recently, Xu et al.<sup>[80]</sup> have developed fluorescent probes NAP-DCP-1 and NAP-DCP-3, which have shown a notable enhancement in reaction rate with methylglyoxal (MGO). The binding process with MGO can be accomplished within a short duration of 20 min, thereby reducing the time required for sample preparation. Furthermore, these probes demonstrate improved selectivity toward MGO, effectively mitigating the impact of potential interfering compounds. These probes have been effectively utilized for the real-time monitoring of MGO levels in tissues and blood samples.

To summarize, fluorescence spectroscopy offers an effective approach for detecting low-concentration  $\alpha$ -DCs in organisms. Its advantages include visualization, specificity, high resolution, high sensitivity, noninvasiveness, and nondestructiveness. However, this method faces a challenge in detecting deep tissues with both high sensitivity and

**Table 5.** Comparison of typical fluorescence (FL) probes for  $\alpha$ -dicarbonyl compounds.

FL probe	FL detection	Biological matrix	Sensitivity (LOD <sup>†</sup> )	Selectivity <sup>†</sup>	References
MBo	$\lambda_{\text{ex/em}} = 480/532$ nm (turn-on)	Hela cells	50 – 100 nM (MGO)	MGO over GO/NO	Wang et al. <sup>[72]</sup>
PDN-1	$\lambda_{\text{ex/em}} = 405/528$ nm $\lambda_{\text{ex/em}} = 880/480-550$ nm	Hela cells	77 nM (MGO)	MGO over GO/NO/MI	Tang et al. <sup>[73]</sup>
NAP-DCP-4	$\lambda_{\text{ex/em}} = 365/559$ nm (irreversible turn-on response, Off-On-Off) $\lambda_{\text{ex/em}} = 425/559$ nm (reversible turn-on response, Off-On-Off)	RAW264.7 cells	1.8 $\mu$ M (MGO)	MGO over GO/NO/MI; FL turn-on ratios: 24.7-fold (MGO), 9.8-fold (GO)	Wang et al. <sup>[74]</sup>
ANC-DCP-1	$\lambda_{\text{ex/em}} = 525/558-615$ nm (turn-on)	Diabetic urine	12.6 $\mu$ M (MGO) 12.1 $\mu$ M (GO)	MGO and GO over NO/FA; FL turn-on ratios: 6.4-fold (MGO), 8.9-fold (GO)	Chen et al. <sup>[48]</sup>
DAN	$\lambda_{\text{ex/em}} = 336/387$ nm $\lambda_{\text{ex/em}} = 365/544$ nm (ratiometric)	HSF cells	0.33 $\mu$ M (MGO)	MGO over GO/NO/FA	Xie et al. <sup>[75]</sup>
DAF-2	$\lambda_{\text{ex/em}} = 435/510$ nm (turn-on)	Human plasma	0.7 $\mu$ M (MGO)	Cross-reactivity with NO	Shaheen et al. <sup>[76]</sup>
NI-OPD	$\lambda_{\text{ex/em}} = 380/460$ nm $\lambda_{\text{ex/em}} = 780/420-480$ nm	HeLa cells	0.56 nM (MGO)	MGO over GO/NO/FA	Yang et al. <sup>[77]</sup>
CMFP	$\lambda_{\text{ex/em}} = 350/440-525$ nm (ratiometric)	HeLa cells Diabetic serum	0.5 $\mu$ M (MGO)	MGO over GO/NO/FA	Wang et al. <sup>[78]</sup>
NP	$\lambda_{\text{ex/em}} = 440/555$ nm $\lambda_{\text{ex/em}} = 760/500-550$ nm	HeLa cells	1.47 $\mu$ M (MGO)	MGO over NO/FA/MI	Gao et al. <sup>[79]</sup>
NAP-DCP-1	$\lambda_{\text{ex/em}} = 425/564$ nm (turn-on)	Diabetic serum	0.72 $\mu$ M (MGO) 0.58 $\mu$ M (GO)	MGO and GO over NO/FA/MI	Xu et al. <sup>[80]</sup>
NAP-DCP-3	$\lambda_{\text{ex/em}} = 425/530-590$ nm (turn-on)	HeLa cells	0.13 $\mu$ M (MGO) 0.16 $\mu$ M (GO)	MGO and GO over NO/FA/MI	

<sup>†</sup>LOD: limit of detection; NO: nitric oxide, an important gas signaling molecule and oxidative stress regulator; FA: formaldehyde, a key intermediate in one-carbon metabolism; MI: metal ions.

resolution due to its susceptibility to environmental factors.<sup>[81]</sup> To address this challenge, current research focuses on developing ratiometric fluorescence probes with emission in the near infrared region to enhance penetration depth and reduce autofluorescence in biological samples.<sup>[82,83]</sup> Current academic research primarily focuses on MGO, with limited exploration of GO and other dicarbonyl compounds. Future efforts could involve designing specialized fluorescence probes for selective recognition of these compounds, advancing dynamic monitoring technologies. Combining

findings from different  $\alpha$ -DCs research could enhance understanding of sugar metabolism products in the human body.

### ***Infrared spectroscopy detection***

The absorption of specific wavelengths of infrared radiation by a molecule results in the transition between vibrational and rotational energy levels. Infrared spectroscopy leverages this phenomenon to furnish insights into the structure and composition of molecules. This technique can be categorized into four types: near-infrared spectroscopy (NIR, wavelength region: 0.75–2.5  $\mu\text{m}$ ), mid-infrared spectroscopy (MIR, wavelength region: 2.5–25  $\mu\text{m}$ ), far-infrared spectroscopy (FIR, wavelength region: 25–1000  $\mu\text{m}$ ), and terahertz spectroscopy (THz, wavelength region: 30–3000  $\mu\text{m}$ ).

### ***NIR spectroscopy detection***

NIR spectroscopy exhibits sensitivity to combination bands arising from fundamental vibrations, particularly those involving H-containing functional groups (C-H, O-H, and N-H). Its nondestructive nature, transparency to water, and swift data acquisition render NIR spectroscopy a versatile analytical tool. However, the direct interpretation of NIR spectra presents challenges due to overlapping bands. To overcome this obstacle, chemometrics have been employed to extract meaningful information from these overlapping NIR bands.<sup>[84]</sup> This combined approach has gained widespread acceptance across diverse applications, ranging from compound composition analysis to quantitative monitoring.<sup>[85,86]</sup> As a typical work within this research domain, Bonapace et al.<sup>[49]</sup> used NIR spectroscopy, principal component analysis and machine learning algorithm to evaluate the concentrations of MGO adducts in cancer cells. The study encompassed a cohort comprising 20 healthy volunteers and 40 cancer patients, with cell samples derived from various biological fluids, including plasma, serum, interstitial fluid, and whole blood. Results demonstrated a high sensitivity to MGO adducts (LOD of 0.03% v/v) and remarkable repeatability in distinguishing between tumor and non-tumor patients (R value of 0.72%) with no instances of false negatives or positives. Notably, this approach stands out for its simplicity and efficiency, relying solely on the direct measurement of solutes remaining on the sample surface after evaporation, thereby obviating the need for sample pretreatment.

In the field of high-contrast imaging, NIR probes have emerged as a novel tool for analyzing  $\alpha$ -DCs in deep tissues (Table 6). These probes can generate signals within the NIR window, thereby mitigating the challenges posed by tissue absorption and scattering under ultraviolet excitation.<sup>[92]</sup> NIR probes are classified into two types based on their emission wavelengths: NIR-I probes (700–900 nm) and NIR-II probes (1000–1700 nm). In 2019, the first NIR-I fluorescent probe (MEBTD) for MGO was proposed by Ding et al.<sup>[46]</sup> The probe incorporated a specially designed thiadiazole-fused OPD moiety, resulting in emission within the range of 600–700 nm. The probe demonstrated several advantages, including a LOD of 18 nM and an off-on ratio of 131-fold. As a result, it was able to effectively visualize and analyze MGO in cancer cells. In 2020, Dang et al.<sup>[87]</sup> designed another NIR-I fluorescent probe (DBTPP), which emitted a signal at 650 nm. This probe exhibited an LOD of 262 nM for MGO, minimal

**Table 6.** Comparison of NIR fluorescence probes for  $\alpha$ -dicarbonyl compounds.

NIR probe	Detection condition	Max penetration depth	Biological matrix	Sensitivity(LOD <sup>†</sup> )	Selectivity <sup>†</sup>	References
MEBTD	$\lambda_{\text{ex/em}} = 496/650$ nm (NIR-I)	N. A.	4T1 tumor	18 nM (MGO)	MGO over GO/ FA/NO FL turn-on ratios: 131-fold (MGO)	Ding et al. <sup>[46]</sup>
DBTPP	$\lambda_{\text{ex/em}} = 500/650$ nm (NIR-I)	N. A.	SH-SY5Y cells	262 nM (MGO)	MGO over GO/ FA/MI; Cross- reactivity with NO in acidic surroundings only	Dang et al. <sup>[87]</sup>
D/I-PNTs	$\lambda_{\text{ex/em}} = 488/820$ nm (NIR-I)	4 mm	4T1 tumor	272 nM (MGO)	MGO over GO/ FA/NO	Liu et al. <sup>[88]</sup>
MG-SLNP	$\lambda_{\text{ex/em}} = 808/1046$ nm (NIR-II)	5 mm	Diabetic blood; Mice kidney	57 nM (MGO)	MGO over GO/ FA/NO/MI	Dang et al. <sup>[89]</sup>
MAM	$\lambda_{\text{ex/em}} = 808/1050$ nm (NIR-II)	N. A.	Mice brain	72 nM (MGO)	MGO over GO/ FA/NO/MI	Lai et al. <sup>[90]</sup>
MRM	$\lambda_{\text{ex/em}} = 808/1048$ nm (NIR-II)	N. A.	4T1 tumor	62 nM (MGO)	MGO over GO/ FA/NO	Lai et al. <sup>[91]</sup>

<sup>†</sup>LOD: limit of detection; NO: nitric oxide, an important gas signaling molecule and oxidative stress; MI: metal ions; N. A. not mentioned in the literature.

autofluorescence, and excellent photostability, enabling *in vivo* visualization of MGO in an Alzheimer's disease mouse. Recently, Liu et al.<sup>[88]</sup> reported a novel NIR-I nanoprobe D/I-PNTs. This probe was prepared by encapsulating the hydrophobic DBTPP probe<sup>[87]</sup> and a hydrophilic IR783 probe into peptide nanotubes. The peptide nanotubes aided in enhancing water solubility, extending the emission range, and obviating the need for complex molecular design and synthesis. Compared to conventional imaging, the resultant nanoprobe exhibited remarkable sensitivity to MGO in deep tissues, with a LOD of 272 nM and a penetration depth of 4 mm. NIR-II probes, which emit in the second near-infrared region, offer an additional approach to enhancing penetration depth. In 2022, Dang et al.<sup>[89]</sup> introduced a novel NIR-II nanoprobe MG-SLNP, by incorporating a specially designed fluorescence probe TDTCD, with an amphiphilic copolymer, lecithin, and solid phase-change materials. This nanoprobe exhibited excellent stability and a high fluorescence quantum yield at emission wavelengths of 808 nm, enabling efficient imaging of MGO in both whole blood and tumor tissues simultaneously. In comparison to traditional imaging methods, this approach demonstrated a high-resolution viewing window, quick response (within 20 min), good penetration depth (5 mm), satisfactory sensitivity (57 nm) and selectivity.

These investigations provide evidence for the viability of NIR techniques in the detection of  $\alpha$ -dicarbonyl compounds within organics, demonstrating their great potential in disease pathology studies and early diagnosis. Current research primarily uses NIR probes to detect MGO, focusing on improving selective identification using OPD as the core reactive group. Introducing heterocyclic structures helps shift emission wavelength to NIR region and increase intensity, enhancing resolution and detection depth.

Nanocapsulation technology is also used to encapsulate NIR probes with hydrophilic materials, improving solubility and bioactivity. To sum up, these near-infrared probes demonstrate exceptional specificity for MGO, highlighting distinct benefits in tissue imaging and continuous blood monitoring. Subsequent research avenues could explore the application of near-infrared probes for additional dicarbonyl compounds, with a focus on adjusting the emission wavelength toward the near-infrared second window to improve detection capabilities at greater depths.

### ***MIR spectroscopy***

In contrast to NIR spectroscopy, MIR spectroscopy primarily corresponds to the fundamental vibrations of chemical bonds, specifically the stretching and bending vibrations. In  $\alpha$ -dicarbonyl compound analysis, MIR characteristic peaks provided useful information for studying their conformation and molecular behavior. In a study conducted by Profeta et al.,<sup>[93]</sup> high-resolution MIR spectroscopy was employed to investigate the vibration modes of GO, MGO, and 2,3-BD for the first time. The results revealed that GO in equilibrium demonstrated a trans configuration with 12 normal modes. MGO exhibited  $C_s$  symmetry and displayed 21 fundamental modes. 2,3-BD featured  $C_{2h}$  symmetry and displayed 30 fundamental modes. Nevertheless, there were inconsistencies between experimental data and theoretical predictions in the 2,3-BD analysis. To address this issue, Gómez-Zavaglia and Fausto<sup>[94]</sup> employed low-temperature solid-state MIR spectroscopy and density functional theory (DFT) calculations to investigate the configuration of 2,3-BD in various phases. They discovered a new conformation for 2,3-BD and clarified the inconsistencies observed in previous research. Through refining the theoretical conformation model for 2,3-BD, they achieved a more accurate prediction of dipole moments in 2,3-BD at different temperatures. In 2016, Leicht et al.<sup>[45]</sup> used MIR spectroscopy and DFT calculations to analyze the configuration of the GO cation, and revealed that the GO cation was only stable in the trans configuration. These works emphasized the importance of MIR spectroscopy in understanding the intricate molecular behavior and properties of  $\alpha$ -DCs.

### ***Fingerprint spectroscopy detection (FIR spectroscopy and THz spectroscopy)***

FIR spectroscopy and THz spectroscopy are sensitive to low-frequency vibrations, including pure rotational transitions, variable-angle vibrations, skeleton vibrations, and lattice vibrations.<sup>[95–98]</sup> In  $\alpha$ -DCs analysis, the characteristic peaks in the far-infrared and terahertz regions provided useful information for studying their aggregation structure and intermolecular interaction. The FIR spectrum of trans-MGO has been examined in detail by Gurnick et al.<sup>[99]</sup> and ensuing works on the vibrational and rotational transitions at lower frequencies of MGO by Huber et al.,<sup>[100]</sup> Profeta et al.,<sup>[93]</sup> and Bteich et al.<sup>[101]</sup> detail the finer rotational and torsional modes overlaying these transitions, especially the effects of rotor-vibrational coupling with the methyl rotor. However, the quantitative detection of  $\alpha$ -DCs within the FIR and THz spectrums presents a significant challenge due to their intrinsic characteristics. Specifically, their absorption peaks are neither sharp nor intense, particularly at lower concentrations. Such limitations impede the direct and accurate detection of  $\alpha$ -DCs through

conventional FIR and THz spectroscopy methods. To address this issue, Wu et al.<sup>[102,103]</sup> introduced an innovative approach. Through the utilization of OPD, MGO underwent a chemical conversion, resulting in a new product with distinct and robust absorption peaks in the far-infrared and terahertz range. This conversion enhanced the sensitivity of MGO detection, enabling quantitative analysis. The method established a linear relationship between MGO concentration and the peak intensity of the reaction product, covering a wide detectable range from 5 to 2500 nmol/mL with exceptional accuracy, as evidenced by a high correlation coefficient of 0.999. This work provides a rapid, straightforward, and cost-effective solution for the early detection and monitoring of diseases linked to MGO levels.

In conclusion, IR spectroscopy is an effective and straightforward method for investigating the molecular structure of  $\alpha$ -DCs. Compared to alternative spectral detection techniques, this analytical method requires a relatively less sample consumption and a shorter analysis time. However, the detection of  $\alpha$ -DCs in organisms poses a challenge due to the overlapping absorption peaks arising from complex compositions. The key to addressing this challenge lies in establishing a robust and accurate analysis model. Ongoing research focuses on advancing the integration of chemometrics and IR spectroscopy analysis to enhance efficacy and precision in identifying information in biological samples.<sup>[104]</sup> Furthermore, researchers are devoted to incorporating these IR analysis models into portable electronic devices for point-of-care testing and remote patient monitoring, thereby expanding the applicability of IR techniques in diverse clinical settings.

### **Nuclear magnetic resonance (NMR) detection**

Nuclear magnetic resonance (NMR) is a physical phenomenon in which nuclei in an external magnetic field absorb and re-emit electromagnetic radiation due to Zeeman splitting resonance. The NMR frequency is in the range of 60–1000 MHz, determined by the magnetic property and the chemical environment of the nuclei. As a result, by tracking the changes in frequency, researchers can identify the chemical structure, molecular dynamics, and intermolecular interaction of analytes.<sup>[105]</sup> The application of NMR spectroscopy in the identification of  $\alpha$ -DCs can be categorized into three distinct areas: structural identification, quantitative analysis, and kinetic analysis of chemical reactions.

In the field of structural identification, NMR spectroscopy offers a noninvasive and precise analytical technique. The earliest research on identifying the structure of  $\alpha$ -DCs was published in 1988. Creighton et al.<sup>[106]</sup> used an 80 MHz NMR spectrometer to study the structure of MGO hydrate. The  $^1\text{H}$  NMR spectrum showed four distinct signals for MGO in  $\text{D}_2\text{O}$ , located at 1.38 ( $^3\text{H}$ ), 2.31 ( $^3\text{H}$ ), 4.82 ( $^1\text{H}$ ), and 5.27 ( $^1\text{H}$ ) ppm respectively. The signals at 2.31 ( $^3\text{H}$ ) ppm and 4.82 ( $^1\text{H}$ ) ppm were attributed to aldehydrol, while the others (1.38 ( $^3\text{H}$ ) and 5.27 ( $^1\text{H}$ ) ppm) were assigned to dihydrate. The ratio of aldehydrol to dihydrate could be determined by comparing their signal intensities, which was found to be approximately 58-62%:38-44%. This allowed for elucidation of the structural conformation of MGO in  $\text{D}_2\text{O}$ . In 2004, Nemet et al.<sup>[47]</sup> investigated the structural differences of MGO in water and organic solvents using  $^1\text{H}$  and  $^{13}\text{C}$  NMR

chemical shifts. The results revealed that MGO predominantly existed as a monomer in the organic solvent (dimethylsulfoxide, DMSO), with characteristic NMR shifts observed at 2.10, 3.30, 4.55 ( $^1\text{H}$ , ppm) and 25.3, 54.5, 103.5, 203.6 ( $^{13}\text{C}$ , ppm). Moreover, upon dissolving freeze-dried MGO in  $\text{D}_2\text{O}$ , these NMR signals obviously shifted in both the  $^1\text{H}$  and  $^{13}\text{C}$  NMR spectra, indicating the formation of double bond couplings between methyl protons and quaternary C-atoms. These findings imply that varying water content in solvents can modulate the structure of MGO leading to transformation from less reactive non-carbonyl form to more reactive carbonyl and dicarbonyl forms. In 2016, Salus et al.<sup>[107]</sup> used NMR technology and DFT-GIAO quantum chemical calculations to investigate the structures of malonaldehyde-glyoxal and malonaldehyde-methylglyoxal etheno adducts in DNA modification. The averaging of  $^1\text{H}$  and  $^{13}\text{C}$  NMR chemical shifts indicated rapid proton transfer between both enol forms of the compounds due to a low energy barrier in the  $\beta$ -dicarbonyl system. These works provided insights into understanding variations in MGO reactivity across different biochemical systems.

In the field of quantitative analysis, Donarski et al.<sup>[108]</sup> pioneered the use of NMR technology in 2010 to quantify MGO concentrations in various foods. By utilizing NMR signals from MGO monohydrate (2.306 and 5.287 ppm) and dihydrate (1.378 ppm), MGO concentration were determined, with a LOD of 11 mg/L and a reliability of 95.4%. Compared to the LC-MS method, NMR spectroscopy proved more efficient as it eliminated the need for chromatographic separation or derivatization procedures. However, traditional NMR techniques face challenges when quantitatively analyzing complex samples. To address this issue, current efforts focus on improving instrumental systems and optimizing analysis algorithms. In 2012, Gresley et al.<sup>[109]</sup> utilized diffusion ordered spectroscopy (DOSY) NMR technology to quantify the MGO concentration in 8 commercial manuka honeys. This approach enabled obtaining relevant information from samples within an hour using high-resolution NMR instrumentation, with a sensitivity ranging from 1.3 to 7.5 ppm. On the other another hand, Spiteri et al.<sup>[110]</sup> integrated NMR technology with chemometrics (principal components analysis, PCA) for analyzing the MGO content in 250 types of honey. This amalgamation proved valuable for rapidly distinguishing Manuka honey from other Oceania floral honeys, achieving an accuracy rate of up to 100%.

In the field of chemical reaction kinetics research involving  $\alpha$ -DCs, NMR is extensively applied, particularly in investigating organic aerosol formation with GO. In 2009, Haan et al.<sup>[111]</sup> employed  $^1\text{H}$  and  $^{13}\text{C}$  NMR techniques to examine the reaction processes between GO and five amino acids. The active form fractions, intermediate products, and final reaction products were analyzed using NMR technology to further elucidate the kinetics associated with amino acid loss during reactions with glyoxal at room temperature. This study demonstrates that the vapor GO reaction in aerosols can persist for several months, but the conversion of GO dihydrate to its reactive monohydrate can be induced by drying, resulting in a significant reduction in reaction time. In 2015, Maxut et al.<sup>[112]</sup> investigated the reaction process of spontaneous imidazole synthesis from glyoxal using NMR techniques. They analyzed the structures and yields of GO oligomers and intermediate products under different pH conditions, revealing a kinetic competition between the pathway for imidazole formation and the pathway for acetal/oligomer formation in GO self-reaction. This study identifies a bottleneck in

achieving higher imidazole formation in environmentally friendly ammonium aqueous solutions at neutral pH. In 2016, Alexis et al.<sup>[113]</sup> used NMR spectroscopy to monitor the aqueous photochemistry process of GO and glyoxylic acid. Based on the  $^{13}\text{C}$  NMR peak at 93.22 ppm, which corresponds to GO, the source of GO and the related reaction mechanism of the photolysis of secondary organic aerosols were eventually revealed.

To sum up, it can be said that NMR spectroscopy is unquestionably a leading technique for fine structure analysis of  $\alpha$ -DCs at relatively low concentrations (ppm levels). This is the only experimental method capable of determining the three-dimensional structure of  $\alpha$ -DCs in solution systems. However, the NMR instruments are always large, expensive, and requires high technical proficiency for analysis, which limits its use outside of laboratories. To overcome this limitation, future development aims to miniaturize NMR instruments (such as NMR-on-a-chip)<sup>[114]</sup> and integrate chemometrics to simplify the data analysis process.<sup>[115]</sup> These approaches aim to expand the applications of NMR technology beyond atmospheric and food media research, potentially including studies on pharmaceutical and biochemical dynamic processes.

## Conclusion

In the last decade, given the significance of  $\alpha$ -dicarbonyl compounds in disease research and food safety, multiple research groups have explored diverse approaches for detecting  $\alpha$ -dicarbonyl compounds. Most detections employ classic fluorescent spectrum detection techniques, renowned for their high specificity, low detection limit, simplicity, and cost-effectiveness. Ongoing innovative research on fluorescent probes, combined with near-infrared spectroscopy and fluorescence imaging, consistently improves and proposes enhanced detection technologies. Additionally, UV spectroscopy excels in directly identifying  $\alpha$ -dicarbonyl compounds through their inherent UV absorption properties. Its ease of operation allows seamless integration with HPLC, significantly improving accuracy in detecting dicarbonyl compounds in complex mixtures. NMR spectroscopy excels in fine structure analysis, while IR spectrum detection enables both qualitative and quantitative analysis of  $\alpha$ -dicarbonyl compounds based on molecular characteristic vibrations. Collectively, spectral detection techniques for  $\alpha$ -dicarbonyl compounds now offer substantial benefits for human health, disease treatment, and food safety. Ongoing research has introduced simpler, quicker, and more economical technologies for detecting  $\alpha$ -dicarbonyl compounds, with potential applications in clinical and fundamental scientific research, as well as daily life.

## Disclosure statement

No potential conflict of interest was reported by the author(s).

## Funding

This work was supported by the National Key Research and Development Program of China under Grant 2022YFA1404004 and 2023YFF0719200; and the National Natural Science Foundation of China under Grant 61805140, 62335012, and 61988102.

## References

1. Liu, Y.; Lu, L.; Yuan, S.; Guo, Y.; Yao, W.; Zhou, W.; Yu, H. Formation of Advanced Glycation End-Products and  $\alpha$ -Dicarbonyl Compounds through Maillard Reaction: Solutions from Natural Polyphenols. *J. Food Compos. Anal.* **2023**, *120*, 105350. DOI: [10.1016/j.jfca.2023.105350](https://doi.org/10.1016/j.jfca.2023.105350).
2. Rabbani, N.; Thornalley, P. J. Methylglyoxal, Glyoxalase 1 and the Dicarbonyl Proteome. *Amino Acids.* **2012**, *42*, 1133–1142. DOI: [10.1007/s00726-010-0783-0](https://doi.org/10.1007/s00726-010-0783-0).
3. Henning, C.; Liehr, K.; Girndt, M.; Ulrich, C.; Glomb, M. A. Extending the Spectrum of  $\alpha$ -Dicarbonyl Compounds in Vivo\*. *J. Biol. Chem.* **2014**, *289*, 28676–28688. DOI: [10.1074/jbc.M114.563593](https://doi.org/10.1074/jbc.M114.563593).
4. Videira, P. A. Q.; Castro-Caldas, M. Linking Glycation and Glycosylation with Inflammation and Mitochondrial Dysfunction in Parkinson's Disease. *Front. Neurosci.* **2018**, *12*, 381. DOI: [10.3389/fnins.2018.00381](https://doi.org/10.3389/fnins.2018.00381).
5. Allaman, I.; Bélanger, M.; Magistretti, P. J. Methylglyoxal, the Dark Side of Glycolysis. *Front. Neurosci.* **2015**, *9*, 23. DOI: [10.3389/fnins.2015.00023](https://doi.org/10.3389/fnins.2015.00023).
6. Kuntz, S.; Kunz, C.; Rudloff, S. Carbonyl Compounds Methylglyoxal and Glyoxal Affect Interleukin-8 Secretion in Intestinal Cells by Superoxide Anion Generation and Activation of MAPK p38. *Mol. Nutr. Food Res.* **2010**, *54*, 1458–1467. DOI: [10.1002/mnfr.200900408](https://doi.org/10.1002/mnfr.200900408).
7. Svendsen, C.; Høie, A. H.; Alexander, J.; Murkovic, M.; Husøy, T. The Food Processing Contaminant Glyoxal Promotes Tumour Growth in the Multiple Intestinal Neoplasia (Min) Mouse Model. *Food Chem. Toxicol.* **2016**, *94*, 197–202. DOI: [10.1016/j.fct.2016.06.006](https://doi.org/10.1016/j.fct.2016.06.006).
8. Price, C. L.; Knight, S. C. Methylglyoxal: Possible Link between Hyperglycaemia and Immune Suppression? *Trends Endocrinol. Metab.* **2009**, *20*, 312–317. DOI: [10.1016/j.tem.2009.03.010](https://doi.org/10.1016/j.tem.2009.03.010).
9. Wang, W.; Yagiz, Y.; Buran, T. J.; Nunes, C.; Gu, L. Phytochemicals from Berries and Grapes Inhibited the Formation of Advanced Glycation End-Products by Scavenging Reactive Carbonyls. *Food Res. Int.* **2011**, *44*, 2666–2673. DOI: [10.1016/j.microc.2018.05.006](https://doi.org/10.1016/j.microc.2018.05.006).
10. Nokin, M.-J.; Durieux, F.; Bellier, J.; Peulen, O.; Uchida, K.; Spiegel, D. A.; Cochrane, J. R.; Hutton, C. A.; Castronovo, V.; Bellahçène, A. Hormetic Potential of Methylglyoxal, a Side-Product of Glycolysis, in Switching Tumours from Growth to Death. *Sci. Rep.* **2017**, *7*, 11722. DOI: [10.1038/s41598-017-12119-7](https://doi.org/10.1038/s41598-017-12119-7).
11. Leone, A.; Nigro, C.; Nicolò, A.; Prevezano, I.; Formisano, P.; Beguinot, F.; Miele, C. The Dual-Role of Methylglyoxal in Tumor Progression – Novel Therapeutic Approaches. *Front. Oncol.* **2021**, *11*, 645686. DOI: [10.3389/fonc.2021.645686](https://doi.org/10.3389/fonc.2021.645686).
12. Perween, S.; Abidi, M.; Faizy, A. F.; Moinuddin. Post-Translational Modifications on Glycated Plasma Fibrinogen: A Physicochemical Insight. *Int. J. Biol. Macromol.* **2019**, *126*, 1201–1212. DOI: [10.1016/j.ijbiomac.2019.01.018](https://doi.org/10.1016/j.ijbiomac.2019.01.018).
13. Kovacic, P.; Cooksy, A. L. Electron Transfer as a Potential Cause of Diacetyl Toxicity in Popcorn Lung Disease. In *Reviews of Environmental Contamination and Toxicology*; Whitacre, D. M., Ed.; Springer New York: New York, **2010**; pp 133–148.
14. Fennell, T. R.; Morgan, D. L.; Watson, S. L.; Dhungana, S.; Waidyanatha, S. Systemic Uptake, Albumin and Hemoglobin Binding of [ $^{14}\text{C}$ ]2,3-Butanedione Administered by Intratracheal Instillation in Male Harlan Sprague Dawley Rats and Oropharyngeal Aspiration in Male B6C3F1/N Mice. *Chem. Biol. Interact.* **2015**, *227*, 112–119. DOI: [10.1016/j.cbi.2014.12.029](https://doi.org/10.1016/j.cbi.2014.12.029).
15. Ashraf, J. M.; Shahab, U.; Tabrez, S.; Lee, E. J.; Choi, I.; Aslam Yusuf, M.; Ahmad, S. DNA Glycation from 3-Deoxyglucosone Leads to the Formation of AGEs: Potential Role in Cancer Auto-Antibodies. *Cell Biochem. Biophys.* **2016**, *74*, 67–77. DOI: [10.1007/s12013-015-0713-6](https://doi.org/10.1007/s12013-015-0713-6).

16. Ashraf, J. M. 3-Deoxyglucosone as a Potential Agent That Alters IgG Protein through Advanced Glycation End Products. *Appl. Biochem. Microbiol.* **2021**, *57*, 468–474. DOI: [10.1134/S0003683821040025](https://doi.org/10.1134/S0003683821040025).
17. Wang, Y.; Ho, C.-T. Dicarbonyl Intermediates: A Control Factor in the Maillard Reaction. In *Controlling Maillard Pathways to Generate Flavors*; Mottram, D. S., Taylor, A. J.; American Chemical Society: Washington, DC, **2010**; pp. 27–34.
18. Baba, S. P.; Barski, O. A.; Ahmed, Y.; O'Toole, T. E.; Conklin, D. J.; Bhatnagar, A.; Srivastava, S. Reductive Metabolism of AGE Precursors: A Metabolic Route for Preventing AGE Accumulation in Cardiovascular Tissue. *Diabetes* **2009**, *58*, 2486–2497. DOI: [10.2337/db09-0375](https://doi.org/10.2337/db09-0375).
19. Sheng, C. S.; Tian, J.; Miao, Y.; Cheng, Y.; Yang, Y.; Reaven, P. D.; Bloomgarden, Z. T.; Ning, G. Prognostic Significance of Long-Term HbA(1c) Variability for All-Cause Mortality in the ACCORD Trial. *Diabetes Care*. **2020**, *43*, 1185–1190. DOI: [10.2337/dc19-2589](https://doi.org/10.2337/dc19-2589).
20. Bierhaus, A.; Fleming, T.; Stoyanov, S.; Leffler, A.; Babes, A.; Neacsu, C.; Sauer, S. K.; Eberhardt, M.; Schnölzer, M.; Lasitschka, F.; et al. Methylglyoxal Modification of Nav1.8 Facilitates Nociceptive Neuron Firing and Causes Hyperalgesia in Diabetic Neuropathy. *Nat. Med.* **2012**, *18*, 926–933. DOI: [10.1038/nm.2750](https://doi.org/10.1038/nm.2750).
21. Rodrigues, D. C.; Harvey, E. M.; Suraj, R.; Erickson, S. L.; Mohammad, L.; Ren, M.; Liu, H.; He, G.; Kaplan, D. R.; Ellis, J.; et al. Methylglyoxal Couples Metabolic and Translational Control of Notch Signalling in Mammalian Neural Stem Cells. *Nat. Commun.* **2020**, *11*, 2018. DOI: [10.1038/s41467-020-15941-2](https://doi.org/10.1038/s41467-020-15941-2).
22. Kuhla, B.; LÜTh, H.-J.; Haferburg, D.; Boeck, K.; Arendt, T.; MÜNch, G. Methylglyoxal, Glyoxal, and Their Detoxification in Alzheimer's Disease. *Ann. N Y Acad. Sci.* **2005**, *1043*, 211–216. DOI: [10.1196/annals.1333.026](https://doi.org/10.1196/annals.1333.026).
23. Lai, S. W. T.; Hernandez-Castillo, C.; De Jesus Lopez Gonzalez, E.; Zoukari, T.; Talley, M.; Paquin, N.; Chen, Z.; Roep, B. O.; Kaddis, J. S.; Natarajan, R.; et al. Methylglyoxal Adducts Are Prognostic Biomarkers for Diabetic Kidney Disease in Patients with Type 1 Diabetes. *Diabetes* **2023**, *73*, 611–617. DOI: [10.2337/db23-0277](https://doi.org/10.2337/db23-0277).
24. Alfarouk, K. O.; Alqahtani, S. S.; Alshahrani, S.; Morgenstern, J.; Supuran, C. T.; Reshkin, S. J. The Possible Role of Methylglyoxal Metabolism in Cancer. *J. Enzyme Inhib. Med. Chem.* **2021**, *36*, 2010–2015. DOI: [10.1080/14756366.2021.1972994](https://doi.org/10.1080/14756366.2021.1972994).
25. Cai, W.; Ramdas, M.; Zhu, L.; Chen, X.; Striker, G. E.; Vlassara, H. Oral Advanced Glycation Endproducts (AGEs) Promote Insulin Resistance and Diabetes by Depleting the Antioxidant Defenses AGE Receptor-1 and Sirtuin 1. *Proc. Natl. Acad. Sci. U S A* **2012**, *109*, 15888–15893. DOI: [10.1073/pnas.1205847109](https://doi.org/10.1073/pnas.1205847109).
26. Hanssen, N. M. J.; Westerink, J.; Scheijen, J.; van der Graaf, Y.; Stehouwer, C. D. A.; Schalkwijk, C. G. SMART Study Group. Higher Plasma Methylglyoxal Levels Are Associated with Incident Cardiovascular Disease and Mortality in Individuals with Type 2 Diabetes. *Diabetes Care* **2018**, *41*, 1689–1695. DOI: [10.2337/dc18-0159](https://doi.org/10.2337/dc18-0159).
27. Sankaralingam, S.; Ibrahim, A.; Rahman, M. D. M.; Eid, A. H.; Munusamy, S. Role of Methylglyoxal in Diabetic Cardiovascular and Kidney Diseases: Insights from Basic Science for Application into Clinical Practice. *Curr. Pharm. Des.* **2018**, *24*, 3072–3083. DOI: [10.2174/1381612824666180903141832](https://doi.org/10.2174/1381612824666180903141832).
28. Schalkwijk, C. G.; Stehouwer, C. D. A. Methylglyoxal, a Highly Reactive Dicarbonyl Compound, in Diabetes, Its Vascular Complications, and Other Age-Related Diseases. *Physiol. Rev.* **2020**, *100*, 407–461. DOI: [10.1152/physrev.00001.2019](https://doi.org/10.1152/physrev.00001.2019).
29. Hernandez-Castillo, C.; Shuck, S. C. Diet and Obesity-Induced Methylglyoxal Production and Links to Metabolic Disease. *Chem. Res. Toxicol.* **2021**, *34*, 2424–2440. DOI: [10.1021/acs.chemrestox.1c00221](https://doi.org/10.1021/acs.chemrestox.1c00221).
30. Hanssen, N. M. J.; Stehouwer, C. D. A.; Schalkwijk, C. G. Methylglyoxal Stress, the Glyoxalase System, and Diabetic Chronic Kidney Disease. *Curr. Opin. Nephrol. Hypertens.* **2019**, *28*, 26–33. DOI: [10.1097/mnh.0000000000000465](https://doi.org/10.1097/mnh.0000000000000465).

31. Hipkiss, A. R. On the Relationship between Energy Metabolism, Proteostasis, Aging and Parkinson's Disease: Possible Causative Role of Methylglyoxal and Alleviative Potential of Carnosine. *Aging Dis.* **2017**, *8*, 334–345. DOI: [10.14336/ad.2016.1030](https://doi.org/10.14336/ad.2016.1030).
32. Wei, C. C.; Li, S. W.; Wu, C. T.; How, C. M.; Pan, M. H. Dietary Methylglyoxal Exposure Induces Alzheimer's Disease by Promoting Amyloid  $\beta$  Accumulation and Disrupting Autophagy in *Caenorhabditis elegans*. *J. Agric. Food Chem.* **2022**, *70*, 10011–10021. DOI: [10.1021/acs.jafc.2c03411](https://doi.org/10.1021/acs.jafc.2c03411).
33. Kim, E. S.; Yaylayan, V. Profiling of Glucose Degradation Products through Complexation with Divalent Metal Ions Coupled with ESI/qTOF/MS/MS Analysis. *Curr. Res. Food Sci.* **2020**, *3*, 268–274. DOI: [10.1016/j.crfs.2020.10.001](https://doi.org/10.1016/j.crfs.2020.10.001).
34. Han, Z.-G.; Zhang, L.; Qi, C.; Shi, Q.; Min, J. Z. A Novel Reagent Pre-Column Derivatization Method for UHPLC-MS/MS to Determine Four  $\alpha$ -Dicarbonyl Compounds in Beer. *Eur. Food Res. Technol.* **2023**, *249*, 2017–2027. DOI: [10.1007/s00217-023-04269-y](https://doi.org/10.1007/s00217-023-04269-y).
35. Kocadağlı, T.; Gökmen, V. Investigation of  $\alpha$ -Dicarbonyl Compounds in Baby Foods by High-Performance Liquid Chromatography Coupled with Electrospray Ionization Mass Spectrometry. *J. Agric. Food Chem.* **2014**, *62*, 7714–7720. DOI: [10.1021/jf502418n](https://doi.org/10.1021/jf502418n).
36. Ramachandra Bhat, L.; Vedantham, S.; Krishnan, U. M.; Rayappan, J. B. B. Methylglyoxal – an Emerging Biomarker for Diabetes Mellitus Diagnosis and Its Detection Methods. *Biosens. Bioelectron.* **2019**, *133*, 107–124. DOI: [10.1016/j.bios.2019.03.010](https://doi.org/10.1016/j.bios.2019.03.010).
37. Novak, D.; Viskupicova, J.; Zatloukalova, M.; Heger, V.; Michalikova, S.; Majekova, M.; Vacek, J. Electrochemical Behavior of Sarco/Endoplasmic Reticulum Ca-ATPase in Response to Carbonylation Processes. *J. Electroanal. Chem.* **2018**, *812*, 258–264. DOI: [10.1016/j.jelechem.2018.01.036](https://doi.org/10.1016/j.jelechem.2018.01.036).
38. Kold-Christensen, R.; Jensen, K. K.; Smedegård-Holmquist, E.; Sørensen, L. K.; Hansen, J.; Jørgensen, K. A.; Kristensen, P.; Johannsen, M. ReactELISA Method for Quantifying Methylglyoxal Levels in Plasma and Cell Cultures. *Redox Biol.* **2019**, *26*, 101252. DOI: [10.1016/j.redox.2019.101252](https://doi.org/10.1016/j.redox.2019.101252).
39. Marri, L.; Jansson, A. M.; Christensen, C. E.; Hindsgaul, O. An Enzyme-Linked Immunosorbent Assay for the Detection of Diacetyl (2,3-Butanedione). *Anal. Biochem.* **2017**, *535*, 12–18. DOI: [10.1016/j.ab.2017.07.021](https://doi.org/10.1016/j.ab.2017.07.021).
40. Lohumi, S.; Lee, S.; Lee, H.; Cho, B.-K. A Review of Vibrational Spectroscopic Techniques for the Detection of Food Authenticity and Adulteration. *Trends Food Sci. Technol.* **2015**, *46*, 85–98. DOI: [10.1016/j.tifs.2015.08.003](https://doi.org/10.1016/j.tifs.2015.08.003).
41. Wu, D.; Shi, H.; Wang, S.; He, Y.; Bao, Y.; Liu, K. Rapid Prediction of Moisture Content of Dehydrated Prawns Using Online Hyperspectral Imaging System. *Anal. Chim. Acta.* **2012**, *726*, 57–66. DOI: [10.1016/j.aca.2012.03.038](https://doi.org/10.1016/j.aca.2012.03.038).
42. Kamruzzaman, M.; Barbin, D.; ElMasry, G.; Sun, D.-W.; Allen, P. Potential of Hyperspectral Imaging and Pattern Recognition for Categorization and Authentication of Red Meat. *Innov. Food Sci. Emerg. Technol.* **2012**, *16*, 316–325. DOI: [10.1016/j.ifset.2012.07.007](https://doi.org/10.1016/j.ifset.2012.07.007).
43. Hellwig, M.; Löbmann, K.; Orywol, T.; Voigt, A. Model Studies on the Oxidation of Benzoyl Methionine in a Carbohydrate Degradation System. *J. Agric. Food Chem.* **2014**, *62*, 4425–4433. DOI: [10.1021/jf500733f](https://doi.org/10.1021/jf500733f).
44. Chen, L.; Fu, Y.-J.; Fang, W.-L.; Guo, X.-F.; Wang, H. Screening of a Highly Effective Fluorescent Derivatization Reagent for Carbonyl Compounds and Its Application in HPLC with Fluorescence Detection. *Talanta* **2018**, *186*, 221–228. DOI: [10.1016/j.talanta.2018.04.017](https://doi.org/10.1016/j.talanta.2018.04.017).
45. Leicht, D.; Cheng, T. C.; Duncan, M. A. Infrared Spectroscopy of the Glyoxal Radical Cation: The Charge Dependence of Internal Rotation. *Chem. Phys. Lett.* **2016**, *643*, 89–92. DOI: [10.1016/j.cplett.2015.11.018](https://doi.org/10.1016/j.cplett.2015.11.018).
46. Ding, C.; Wang, F.; Dang, Y.; Xu, Z.; Li, L.; Lai, Y.; Yu, H.; Luo, Y.; Huang, R.; Zhang, A.; Zhang, W. Imaging Tumorous Methylglyoxal by an Activatable near-Infrared Fluorescent Probe for Monitoring Glyoxalase 1 Activity. *Anal. Chem.* **2019**, *91*, 15577–15584. DOI: [10.1021/acs.analchem.9b03600](https://doi.org/10.1021/acs.analchem.9b03600).

47. Nemet, I.; Vikić-Topić, D.; Varga-Defterdarović, L. Spectroscopic Studies of Methylglyoxal in Water and Dimethylsulfoxide. *Bioorg. Chem.* **2004**, *32*, 560–570. DOI: [10.1016/j.bioorg.2004.05.008](https://doi.org/10.1016/j.bioorg.2004.05.008).
48. Chen, J.; Lin, Y.; Xing, W.; Zhang, X.; Xu, H.; Wang, W.; Lou, K. An Anthracenecarboximide-Guanidine Fluorescent Probe for Selective Detection of Glyoxals under Weak Acidic Conditions. *RSC Adv.* **2022**, *12*, 9473–9477. DOI: [10.1039/D2RA00741J](https://doi.org/10.1039/D2RA00741J).
49. Bonapace, G.; Gentile, F.; Coppedé, N.; Coluccio, M. L.; Garo, V.; Vismara, M. F. M.; Candeloro, P.; Donato, G.; Malara, N. Methylglyoxal Adducts Levels in Blood Measured on Dried Spot by Portable near-Infrared Spectroscopy. *Nanomaterials (Basel)* **2021**, *11*, 2432. DOI: [10.3390/nano11092432](https://doi.org/10.3390/nano11092432).
50. Meller, R.; Raber, W.; Crowley, J. N.; Jenkin, M. E.; Moortgat, G. K. The UV-Visible Absorption Spectrum of Methylglyoxal. *J. Photochem. Photobiol. A: Chem.* **1991**, *62*, 163–171. DOI: [10.1016/1010-6030\(91\)87017-P](https://doi.org/10.1016/1010-6030(91)87017-P).
51. Koch, S.; Moortgat, G. K. Photochemistry of Methylglyoxal in the Vapor Phase. *J. Phys. Chem. A* **1998**, *102*, 9142–9153. DOI: [10.1021/jp981915r](https://doi.org/10.1021/jp981915r).
52. Volkamer, R.; Spietz, P.; Burrows, J.; Platt, U. High-Resolution Absorption Cross-Section of Glyoxal in the UV-Vis and IR Spectral Ranges. *J. Photochem. Photobiol. A: Chem.* **2005**, *172*, 35–46. DOI: [10.1016/j.jphotochem.2004.11.011](https://doi.org/10.1016/j.jphotochem.2004.11.011).
53. Nemet, I.; Varga-Defterdarović, L.; Turk, Z. Preparation and Quantification of Methylglyoxal in Human Plasma Using Reverse-Phase High-Performance Liquid Chromatography. *Clin. Biochem.* **2004**, *37*, 875–881. DOI: [10.1016/j.clinbiochem.2004.05.024](https://doi.org/10.1016/j.clinbiochem.2004.05.024).
54. Wang, X.-J.; Gao, F.; Li, L.-C.; Hui, X.; Li, H.; Gao, W.-Y. Quantitative Analyses of  $\alpha$ -Dicarbonyl Compounds in Food Samples by HPLC Using 4-(2,3-Dimethyl-6-Quinoxaliny)-1,2-Benzenediamine as a Derivatizing Reagent. *Microchem. J.* **2018**, *141*, 64–70. DOI: [10.1016/j.microc.2018.05.006](https://doi.org/10.1016/j.microc.2018.05.006).
55. Wang, X.-J.; Zhang, H.-X.; Li, H.; Zhu, A.-H.; Gao, W.-Y. Measurement of  $\alpha$ -Dicarbonyl Compounds in Human Saliva by Pre-Column Derivatization HPLC. *Clin. Chem. Lab. Med.* **2019**, *57*, 1915–1922. DOI: [10.1515/cclm-2019-0350](https://doi.org/10.1515/cclm-2019-0350).
56. Wang, X.-J.; Ma, S.-B.; Liu, Z.-F.; Li, H.; Gao, W.-Y. Elevated Levels of  $\alpha$ -Dicarbonyl Compounds in the Plasma of Type II Diabetics and Their Relevance with Diabetic Nephropathy. *J. Chromatogr. B Analyt. Technol. Biomed. Life Sci.* **2019**, *1106-1107*, 19–25. DOI: [10.1016/j.jchromb.2018.12.027](https://doi.org/10.1016/j.jchromb.2018.12.027).
57. Taïbi, N.; Taïbi, A.; Ameraoui, R.; Abou-Mustapha, M.; Hadjadj, M.; Boutaiba, Z.-M.; Kaced, A.; Djema, S.; Al-Balas, Q.-A.; Al Jabal, G.-A.; et al. Development of Analytical Methods GC-MS vs LC-UV for the Serum Monitoring of an Inflammatory Glycotoxin (Methylglyoxal): a New Biomarker of Bovine Hepatobiliary Distomatosis. *Biochimie* **2020**, *168*, 169–184. DOI: [10.1016/j.biochi.2019.11.002](https://doi.org/10.1016/j.biochi.2019.11.002).
58. Gensberger, S.; Mittelmaier, S.; Glomb, M. A.; Pischetsrieder, M. Identification and Quantification of Six Major  $\alpha$ -Dicarbonyl Process Contaminants in High-Fructose Corn Syrup. *Anal. Bioanal. Chem.* **2012**, *403*, 2923–2931. DOI: [10.1007/s00216-012-5817-x](https://doi.org/10.1007/s00216-012-5817-x).
59. Degen, J.; Hellwig, M.; Henle, T. 1,2-Dicarbonyl Compounds in Commonly Consumed Foods. *J. Agric. Food Chem.* **2012**, *60*, 7071–7079. DOI: [10.1021/jf301306g](https://doi.org/10.1021/jf301306g).
60. Treibmann, S.; Groß, J.; Pätzold, S.; Henle, T. Studies on the Reaction of Dietary Methylglyoxal and Creatine during Simulated Gastrointestinal Digestion and in Human Volunteers. *Nutrients* **2022**, *14*, 3598. DOI: [10.3390/nu14173598](https://doi.org/10.3390/nu14173598).
61. Kertsch, A.-L.; Wagner, J.; Henle, T. Selected Maillard Reaction Products and Their Yeast Metabolites in Commercial Wines. *J. Agric Food Chem.* **2023**, *71*, 12300–12310. DOI: [10.1021/acs.jafc.3c04512](https://doi.org/10.1021/acs.jafc.3c04512).
62. Dhar, A.; Desai, K.; Liu, J.; Wu, L. Methylglyoxal, Protein Binding and Biological Samples: Are we Getting the True Measure? *J. Chromatogr. B Analyt. Technol. Biomed. Life Sci.* **2009**, *877*, 1093–1100. DOI: [10.1016/j.jchromb.2009.02.055](https://doi.org/10.1016/j.jchromb.2009.02.055).

63. He, J.; Xie, C.; Meng, C.; Chen, X.; Liu, H.; Sun, B. Molecularly Imprinted Thermosensitive Probe Based on Fluorescent Advanced Glycation End Products to Detect  $\alpha$ -Dicarbonyl Compounds and Inhibit Pyrraline Formation. *Anal. Bioanal. Chem.* **2023**, *415*, 5011–5021. DOI: [10.1007/s00216-023-04787-4](https://doi.org/10.1007/s00216-023-04787-4).
64. Xu, Q.; Yin, Y.; Liu, Y.; Ma, Q.; Chen, X.; Zhao, J. Simultaneous Determination of Six  $\alpha$ -Dicarbonyl Compounds in Traditional Chinese Medicines Using High-Performance Liquid Chromatography-Fluorescence Detector with Pre-Column Derivatization. *J. Sep. Sci.* **2023**, *46*, e2300435. DOI: [10.1002/jssc.202300435](https://doi.org/10.1002/jssc.202300435).
65. Lodge-Ivey, S. L.; May, T.; Petersen, M. K.; Strickland, J. R. Determination of Methylglyoxal in Ruminant Fluid by High-Performance Liquid Chromatography Using Fluorometric Detection. *J. Agric. Food Chem.* **2004**, *52*, 6875–6878. DOI: [10.1021/jf049736w](https://doi.org/10.1021/jf049736w).
66. Ojeda, A. G.; Wrobel, K.; Escobosa, A. R. C.; Garay-Sevilla, M. E.; Wrobel, K. High-Performance Liquid Chromatography Determination of Glyoxal, Methylglyoxal, and Diacetyl in Urine Using 4-Methoxy-o-Phenylenediamine as Derivatizing Reagent. *Anal. Biochem.* **2014**, *449*, 52–58. DOI: [10.1016/j.ab.2013.12.014](https://doi.org/10.1016/j.ab.2013.12.014).
67. Rodríguez-Cáceres, M. I.; Palomino-Vasco, M.; Mora-Diez, N.; Acedo-Valenzuela, M. I. Novel HPLC – Fluorescence Methodology for the Determination of Methylglyoxal and Glyoxal. Application to the Analysis of Monovarietal Wines “Ribera Del Guadiana. *Food Chem.* **2015**, *187*, 159–165. DOI: [10.1016/j.foodchem.2015.04.103](https://doi.org/10.1016/j.foodchem.2015.04.103).
68. Ogasawara, Y.; Tanaka, R.; Koike, S.; Horiuchi, Y.; Miyashita, M.; Arai, M. Determination of Methylglyoxal in Human Blood Plasma Using Fluorescence High Performance Liquid Chromatography after Derivatization with 1,2-Diamino-4,5-Methylenedioxybenzene. *J. Chromatogr. B Analyt. Technol. Biomed. Life Sci.* **2016**, *1029–1030*, 102–105. DOI: [10.1016/j.jchromb.2016.07.019](https://doi.org/10.1016/j.jchromb.2016.07.019).
69. Dhananjayan, K.; Irrgang, F.; Raju, R.; Harman, D. G.; Moran, C.; Srikanth, V.; Münch, G. Determination of Glyoxal and Methylglyoxal in Serum by UHPLC Coupled with Fluorescence Detection. *Anal. Biochem.* **2019**, *573*, 51–66. DOI: [10.1016/j.ab.2019.02.014](https://doi.org/10.1016/j.ab.2019.02.014).
70. Hurtado-Sánchez, M.; Espinosa-Mansilla, A.; Rodríguez-Cáceres, M. I.; Durán-Merás, I. Evaluation of Liquid Chromatographic Behavior of Lumazinic Derivatives, from  $\alpha$ -Dicarbonyl Compounds, in Different C18 Columns: Application to Wine Samples Using a Fused-Core Column and Fluorescence Detection. *J. Agric. Food Chem.* **2014**, *62*, 97–106. DOI: [10.1021/jf404180t](https://doi.org/10.1021/jf404180t).
71. El-Maghrabey, M. H.; Kishikawa, N.; Ohyama, K.; Kuroda, N. Analytical Method for Lipoperoxidation Relevant Reactive Aldehydes in Human Sera by High-Performance Liquid Chromatography-Fluorescence Detection. *Anal. Biochem.* **2014**, *464*, 36–42. DOI: [10.1016/j.ab.2014.07.002](https://doi.org/10.1016/j.ab.2014.07.002).
72. Wang, T.; Douglass, Jr., E. F.; Fitzgerald, K. J.; Spiegel, D. A. A “Turn-on” Fluorescent Sensor for Methylglyoxal. *J. Am. Chem. Soc.* **2013**, *135*, 12429–12433. DOI: [10.1021/ja406077j](https://doi.org/10.1021/ja406077j).
73. Tang, T.; Zhou, Y.; Chen, Y.; Li, M.; Feng, Y.; Wang, C.; Wang, S.; Zhou, X. A Two-Photon Fluorescent Probe for Selective Methylglyoxal Detection and Application in Living Cells. *Anal. Methods* **2015**, *7*, 2386–2390. DOI: [10.1039/C4AY02922D](https://doi.org/10.1039/C4AY02922D).
74. Wang, W.; Chen, J.; Ma, H.; Xing, W.; Lv, N.; Zhang, B.; Xu, H.; Wang, W.; Lou, K. An “and”-Logic-Gate-Based Fluorescent Probe with Dual Reactive Sites for Monitoring Extracellular Methylglyoxal Level Changes of Activated Macrophages. *Chem. Commun. (Camb)* **2021**, *57*, 8166–8169. DOI: [10.1039/d1cc01859k](https://doi.org/10.1039/d1cc01859k).
75. Xie, Q.; Zhan, Y.; Guo, L.; Hao, H.; Shi, X.; Yang, J.; Luo, F.; Qiu, B.; Lin, Z. A Ratiometric Fluorescence Probe for Selective Detection of Ex Vivo Methylglyoxal in Diabetic Mice. *ChemistryOpen* **2022**, *11*, e202200055. DOI: [10.1002/open.202200055](https://doi.org/10.1002/open.202200055).
76. Shaheen, F.; Shmygol, A.; Rabbani, N.; Thornalley, P. J. A Fluorogenic Assay for Methylglyoxal. *Biochem. Soc. Trans.* **2014**, *42*, 548–555. DOI: [10.1042/BST20140028](https://doi.org/10.1042/BST20140028).

77. Yang, M.; Fan, J.; Zhang, J.; Du, J.; Peng, X. Visualization of Methylglyoxal in Living Cells and Diabetic Mice Model with a 1,8-Naphthalimide-Based Two-Photon Fluorescent Probe. *Chem. Sci.* **2018**, *9*, 6758–6764. DOI: [10.1039/C8SC02578A](https://doi.org/10.1039/C8SC02578A).
78. Wang, H.; Xu, Y.; Rao, L.; Yang, C.; Yuan, H.; Gao, T.; Chen, X.; Sun, H.; Xian, M.; Liu, C.; et al. Ratiometric Fluorescent Probe for Monitoring Endogenous Methylglyoxal in Living Cells and Diabetic Blood Samples. *Anal. Chem.* **2019**, *91*, 5646–5653. DOI: [10.1021/acs.analchem.8b05426](https://doi.org/10.1021/acs.analchem.8b05426).
79. Gao, S.; Tang, Y.; Lin, W. Development of a Highly Selective Two-Photon Probe for Methylglyoxal and Its Applications in Living Cells, Tissues, and Zebrafish. *J. Fluoresc.* **2019**, *29*, 155–163. DOI: [10.1007/s10895-018-2323-3](https://doi.org/10.1007/s10895-018-2323-3).
80. Xu, H.; Liu, Q.; Song, X.; Wang, C.; Wang, X.; Ma, S.; Wang, X.; Feng, Y.; Meng, X.; Liu, X.; et al. Fluorophore-Promoted Facile Deprotonation and Exocyclic Five-Membered Ring Cyclization for Selective and Dynamic Tracking of Labile Glyoxals. *Anal. Chem.* **2020**, *92*, 13829–13838. DOI: [10.1021/acs.analchem.0c02447](https://doi.org/10.1021/acs.analchem.0c02447).
81. Kaskova, Z. M.; Tsarkova, A. S.; Yampolsky, I. V. 1001 Lights: Luciferins, Luciferases, Their Mechanisms of Action and Applications in Chemical Analysis, Biology and Medicine. *Chem. Soc. Rev.* **2016**, *45*, 6048–6077. DOI: [10.1039/C6CS00296J](https://doi.org/10.1039/C6CS00296J).
82. Wu, K.; Ma, C.; Wang, Y. Functional Nucleic Acid Probes Based on Two-Photon for Biosensing. *Biosensors. (Basel)* **2023**, *13*, 836. DOI: [10.3390/bios13090836](https://doi.org/10.3390/bios13090836).
83. Huang, X.; Song, J.; Yung, B. C.; Huang, X.; Xiong, Y.; Chen, X. Ratiometric Optical Nanoprobes Enable Accurate Molecular Detection and Imaging. *Chem. Soc. Rev.* **2018**, *47*, 2873–2920. DOI: [10.1039/C7CS00612H](https://doi.org/10.1039/C7CS00612H).
84. Huang, J.; Pu, K. Activatable Molecular Probes for Second near-Infrared Fluorescence, Chemiluminescence, and Photoacoustic Imaging. *Angew. Chem. Int. Ed. Engl.* **2020**, *59*, 11717–11731. DOI: [10.1002/anie.202001783](https://doi.org/10.1002/anie.202001783).
85. Sakudo, A. Near-Infrared Spectroscopy for Medical Applications: Current Status and Future Perspectives. *Clin. Chim. Acta.* **2016**, *455*, 181–188. DOI: [10.1016/j.cca.2016.02.009](https://doi.org/10.1016/j.cca.2016.02.009).
86. Hu, X.; Zuo, Z.; Wang, Y. A Review of the Application of Vibrational Spectroscopy Combined with Chemometrics in Genus *Panax*. *Appl. Spectrosc. Rev.* **2023**, 1–32. DOI: [10.1080/05704928.2023.2211667](https://doi.org/10.1080/05704928.2023.2211667).
87. Dang, Y.; Wang, F.; Li, L.; Lai, Y.; Xu, Z.; Xiong, Z.; Zhang, A.; Tian, Y.; Ding, C.; Zhang, W. An Activatable near-Infrared Fluorescent Probe for Methylglyoxal Imaging in Alzheimer's Disease Mice. *Chem. Commun. (Camb)* **2020**, *56*, 707–710. DOI: [10.1039/C9CC08265D](https://doi.org/10.1039/C9CC08265D).
88. Liu, J.; Li, M.; Dang, Y.; Lou, H.; Xu, Z.; Zhang, W. NIR-I Fluorescence Imaging Tumorous Methylglyoxal by an Activatable Nanoprobe Based on Peptide Nanotubes by FRET Process. *Biosens. Bioelectron.* **2022**, *204*, 114068. DOI: [10.1016/j.bios.2022.114068](https://doi.org/10.1016/j.bios.2022.114068).
89. Dang, Y.; Lai, Y.; Chen, F.; Sun, Q.; Ding, C.; Zhang, W.; Xu, Z. Activatable NIR-II Fluorescent Nanoprobe for Rapid Detection and Imaging of Methylglyoxal Facilitated by the Local Nonpolar Microenvironment. *Anal. Chem.* **2022**, *94*, 1076–1084. DOI: [10.1021/acs.analchem.1c04076](https://doi.org/10.1021/acs.analchem.1c04076).
90. Lai, Y.; Dang, Y.; Sun, Q.; Pan, J.; Yu, H.; Zhang, W.; Xu, Z. Design of an Activatable NIR-II Nanoprobe for the in Vivo Elucidation of Alzheimer's Disease-Related Variations in Methylglyoxal Concentrations. *Chem. Sci.* **2022**, *13*, 12511–12518. DOI: [10.1039/D2SC05242C](https://doi.org/10.1039/D2SC05242C).
91. Lai, Y.; Dang, Y.; Li, F.; Ding, C.; Yu, H.; Zhang, W.; Xu, Z. Reactive Glycolysis Metabolite-Activatable Nanotheranostics for NIR-II Fluorescence Imaging-Guided Phototherapy of Cancer. *Adv. Funct. Materials* **2022**, *32*, 2200016. DOI: [10.1002/adfm.202200016](https://doi.org/10.1002/adfm.202200016).
92. Hong, G.; Antaris, A. L.; Dai, H. Near-Infrared Fluorophores for Biomedical Imaging. *Nat. Biomed. Eng.* **2017**, *1*, 0010. DOI: [10.1038/s41551-016-0010](https://doi.org/10.1038/s41551-016-0010).
93. Profeta, L. T.; Sams, R. L.; Johnson, T. J.; Williams, S. D. Quantitative Infrared Intensity Studies of Vapor-Phase Glyoxal, Methylglyoxal, and 2,3-Butanedione (Diacyetyl) with

- Vibrational Assignments. *J. Phys. Chem. A* **2011**, *115*, 9886–9900. DOI: [10.1021/jp204532x](https://doi.org/10.1021/jp204532x).
94. Gómez-Zavaglia, A.; Fausto, R. Matrix-Isolation and Solid State Low Temperature FT-IR Study of 2,3-Butanedione (Diacetyl). *J. Mol. Struct.* **2003**, *661-662*, 195–208. DOI: [10.1016/j.molstruc.2003.06.003](https://doi.org/10.1016/j.molstruc.2003.06.003).
95. Gong, A.; Qiu, Y.; Chen, X.; Zhao, Z.; Xia, L.; Shao, Y. Biomedical Applications of Terahertz Technology. *Appl. Spectrosc. Rev.* **2020**, *55*, 418–438. DOI: [10.1080/05704928.2019.1670202](https://doi.org/10.1080/05704928.2019.1670202).
96. Peng, Y.; Huang, J.; Luo, J.; Yang, Z.; Wang, L.; Wu, X.; Zang, X.; Yu, C.; Gu, M.; Hu, Q.; et al. Three-Step One-Way Model in Terahertz Biomedical Detection. *PhotonIX* **2021**, *2*, 12. DOI: [10.1186/s43074-021-00034-0](https://doi.org/10.1186/s43074-021-00034-0).
97. Mifsud, D. V.; Hailey, P. A.; Traspas Muiña, A.; Auriacombe, O.; Mason, N. J.; Ioppolo, S. The Role of Terahertz and Far-IR Spectroscopy in Understanding the Formation and Evolution of Interstellar Prebiotic Molecules. *Front. Astron. Space Sci.* **2021**, *8*, 757619. DOI: [10.3389/fspas.2021.757619](https://doi.org/10.3389/fspas.2021.757619).
98. Peng, Y.; Shi, C.; Wu, X.; Zhu, Y.; Zhuang, S. Terahertz Imaging and Spectroscopy in Cancer Diagnostics: A Technical Review. *BME Front.* **2020**, *2020*, 2547609. DOI: [10.34133/2020/2547609](https://doi.org/10.34133/2020/2547609).
99. Gurnick, M.; Chaiken, J.; Benson, T.; McDonald, J. D. Vibrational and Rotational Spectroscopy of the First Electronically Allowed Transition of  $\alpha$ -Dicarbonyls. *J. Chem. Phys.* **1981**, *74*, 99–105. DOI: [10.1063/1.440800](https://doi.org/10.1063/1.440800).
100. Huber, A. S.; Gordon, R. D.; Reid, S. A.; McDonald, J. D. Interaction between Overall and Internal Rotation below, near, and above the Summit of a Torsional Barrier:  $1n\pi^*$  Methylglyoxal. *J. Chem. Phys.* **1992**, *97*, 2338–2346. DOI: [10.1063/1.463125](https://doi.org/10.1063/1.463125).
101. Bteich, S.; Goubet, M.; Motiyenko, R. A.; Margulès, L.; Huet, T. R. Vibrational Dynamic and Spectroscopic Molecular Parameters of trans-Methylglyoxal, a Gaseous Precursor of Secondary Organic Aerosols. *J. Mol. Spectrosc.* **2018**, *348*, 124–129. DOI: [10.1016/j.jms.2017.12.007](https://doi.org/10.1016/j.jms.2017.12.007).
102. Wu, X.; Dai, Y.; Wang, L.; Peng, Y.; Lu, L.; Zhu, Y.; Shi, Y.; Zhuang, S. Diagnosis of Methylglyoxal in Blood by Using Far-Infrared Spectroscopy and o-Phenylenediamine Derivation. *Biomed. Opt. Express.* **2020**, *11*, 963–970. DOI: [10.1364/BOE.381542](https://doi.org/10.1364/BOE.381542).
103. Wu, X.; Peng, Y.; Dai, Y.; Lu, L.; Zhu, Y. High-Risk Factor Detection of Coronary Artery Disease by Terahertz Spectroscopy. 2020 45th International Conference on Infrared, Millimeter, and Terahertz Waves (IRMMW-THz); **2020**; Buffalo, NY: IEEE. DOI: [10.1109/IRMMW-THz46771.2020.9370375](https://doi.org/10.1109/IRMMW-THz46771.2020.9370375).
104. Xuesong, H.; Pu, C.; Jingyan, L.; Yupeng, X.; Dan, L.; Xiaoli, C. Commentary on the Review Articles of Spectroscopy Technology Combined with Chemometrics in the Last Three Years. *Appl. Spectrosc. Rev.* **2023**, 1–60. DOI: [10.1080/05704928.2023.2204946](https://doi.org/10.1080/05704928.2023.2204946).
105. Gerothanassis, I. P.; Troganis, A.; Exarchou, V.; Barbarossou, K. Nuclear Magnetic Resonance (NMR) Spectroscopy: Basic Principles and Phenomena, and Their Applications to Chemistry, Biology and Medicine. *Chem. Educ. Res. Pract* **2002**, *3*, 229–252. DOI: [10.1039/B2RP90018A](https://doi.org/10.1039/B2RP90018A).
106. Creighton, D. J.; Migliorini, M.; Pourmotabbed, T.; Guha, M. K. Optimization of Efficiency in the Glyoxalase Pathway. *Biochemistry* **1988**, *27*, 7376–7384. DOI: [10.1021/bi00419a031](https://doi.org/10.1021/bi00419a031).
107. Salus, K.; Hoffmann, M.; Wyrzykiewicz, B.; Pluskota-Karwatka, D. Structural Studies of Malonaldehyde–Glyoxal and Malonaldehyde–Methylglyoxal Etheno Adducts of Adenine Nucleosides Based on Spectroscopic Methods and DFT-GIAO Calculations. *New J. Chem.* **2016**, *40*, 3875–3884. DOI: [10.1039/C5NJ02835C](https://doi.org/10.1039/C5NJ02835C).
108. Donarski, J. A.; Roberts, D. P. T.; Charlton, A. J. Quantitative NMR Spectroscopy for the Rapid Measurement of Methylglyoxal in Manuka Honey. *Anal. Methods* **2010**, *2*, 1479. DOI: [10.1039/c0ay00125b](https://doi.org/10.1039/c0ay00125b).

109. Gresley, A. L.; Kenny, J.; Cassar, C.; Kelly, A.; Sinclair, A.; Fielder, M. D. The Application of High Resolution Diffusion NMR to the Analysis of Manuka Honey. *Food Chem.* **2012**, *135*, 2879–2886. DOI: [10.1016/j.foodchem.2012.07.072](https://doi.org/10.1016/j.foodchem.2012.07.072).
110. Spiteri, M.; Rogers, K. M.; Jamin, E.; Thomas, F.; Guyader, S.; Lees, M.; Rutledge, D. N. Combination of <sup>1</sup>H NMR and Chemometrics to Discriminate Manuka Honey from Other Floral Honey Types from Oceania. *Food Chem.* **2017**, *217*, 766–772. DOI: [10.1016/j.foodchem.2016.09.027](https://doi.org/10.1016/j.foodchem.2016.09.027).
111. Haan, D. O. D.; Corrigan, A. L.; Smith, K. W.; Stroik, D. R.; Turley, J. J.; Lee, F. E.; Tolbert, M. A.; Jimenez, J. L.; Cordova, K. E.; Ferrell, G. R. Secondary Organic Aerosol-Forming Reactions of Glyoxal with Amino Acids. *Environ. Sci. Technol.* **2009**, *43*, 2818–2824. DOI: [10.1021/es803534f](https://doi.org/10.1021/es803534f).
112. Maxut, A.; Nozière, B.; Fenet, B.; Mechakra, H. Formation Mechanisms and Yields of Small Imidazoles from Reactions of Glyoxal with NH<sub>4</sub><sup>+</sup> in Water at Neutral pH. *Phys. Chem. Chem. Phys.* **2015**, *17*, 20416–20424. DOI: [10.1039/C5CP03113C](https://doi.org/10.1039/C5CP03113C).
113. Eugene, A. J.; Xia, S.-S.; Guzman, M. I. Aqueous Photochemistry of Glyoxylic Acid. *J. Phys. Chem. A* **2016**, *120*, 3817–3826. DOI: [10.1021/acs.jpca.6b00225](https://doi.org/10.1021/acs.jpca.6b00225).
114. Anders, J.; Dreyer, F.; Krüger, D.; Schwartz, I.; Plenio, M. B.; Jelezko, F. Progress in Miniaturization and Low-Field Nuclear Magnetic Resonance. *J. Magn. Reson.* **2021**, *322*, 106860. DOI: [10.1016/j.jmr.2020.106860](https://doi.org/10.1016/j.jmr.2020.106860).
115. de B. Harrington, P.; Wang, X. Spectral Representation of Proton NMR Spectroscopy for the Pattern Recognition of Complex Materials. *J. Anal. Test.* **2017**, *1*, 10. DOI: [10.1007/s41664-017-0003-y](https://doi.org/10.1007/s41664-017-0003-y).